Journal of Volcanology and Geothermal Research 450 (2024) 108086

Contents lists available at ScienceDirect

Journal of Volcanology and Geothermal Research

journal homepage: www.journals.elsevier.com/journal-of-volcanology-and-geothermal-research

Petrogenesis of Miocene volcanism in the Central Anatolia: Geochemical, isotopic and geochronological evidence

Şenel Özdamar [a,*], Mehmet Z. Billor [b], Oral Sarıkaya [a], Bala Ekinci Şans [a], Taşkın Deniz Yıldız [c], Fahri Esenli [a], Haibo Zou [b], Sarah Sherlock [d], Ali Haydar Gültekin [a]

[a] Istanbul Technical University, Department of Geological Engineering, Istanbul 34469, Turkey
[b] Auburn University, College of Sciences and Mathematics, Department of Geosciences, AL 36849, USA
[c] Department of Mining Engineering, Adana Alparslan Türkeş Science and Technology University, Adana, Turkey
[d] STEM Faculty, The Open University, Milton Keynes, UK

ARTICLE INFO

Keywords:
Ar/Ar dating
Central Anatolia
Galatia Volcanic Province
Miocene
Sr-Nd

ABSTRACT

This paper presents the first $^{40}Ar/^{39}Ar$ age data, new bulk-rock major-trace element compositions and Nd—Sr isotope geochemistry, combined with detailed geological mapping of Galatia Volcanic Province (GVP) in the northwest Central Anatolia (Turkey). Here, there are voluminous extrusive rocks in a wide compositional range: a basalt, andesite and trachyte suite, and their pyroclastic equivalents. $^{40}Ar/^{39}Ar$ dating of two whole-rock samples from the GVP yielded plateau ages of 21.76 ± 0.8 Ma and 20.97 ± 0.5 Ma, constrain the volcanic activity at ca. 21 Ma (Aquitanian). The samples show by sub-parallel light rare earth element (LREE)-enrichment and relatively flat heavy rare earth element (HREE) patterns and moderate fractionation [average $(La/Yb)_N$ = 13.5]. Their initial $^{87/86}Sr$ values vary between 0.704619 and 0.704998, while initial $^{143/144}Nd$ values lie between 0.512673 and 0.512755. Integration of the geochemical and geochronological with geological data we propose that the volcanic rocks in the northern area of GVP with calc-alkaline affinity were produced by a lithospheric mantle magma in an extensional setting.

1. Introduction

Anatolia is a part of the Alpine-Himalayan orogenic belt and developed during the evolution of this belt. Miocene volcanic activity in Anatolia produced four subunits: eastern Anatolia, central Anatolia, western Anatolia, and Galatean Volcanic Province (GVP). Of these, GVP comprises a number of Early Miocene volcanic complexes referred as "Kızılcahamam Volcanics" or "Köroğlu Volcanics" (Türkecan, 1991), "Galatia Volcanic Massif" (Gökten et al., 1996) and "Galatean Volcanic Province" (Toprak et al., 1996). The GVP is a widespread volcanosedimentary system between large intra-continental Miocene Beypazarı and Çankırı–Çorum basins (Keller et al., 1992; Toprak et al., 1996; Wilson et al., 1997; Schumacher et al., 2001; Varol et al., 2008). It is an ENE-WSW trending belt bounded in the north by the North Anatolian Fault Zone (NAFZ) and the southern margin is bounded by a lacustrine sedimentary sequence, of Early–Mid-Miocene age, which inter fingers with the volcanics (Toprak et al., 1996). Miocene volcanism in the GVP was divided into two subgroups: 1) Early Miocene, dominated by intermediate-acid lava flows and their pyroclastic equivalents and relatively minor alkali basaltic lava flows and 2) Late Miocene, alkali basalt flows capping the older volcanic sequence (Wilson et al., 1997). There has been no consensus between the different studies, for instance, some studies related the early Miocene volcanism in this region to plate convergence (Tankut, 1990; Keller et al., 1992), whereas new geochemical and Sr—Nd isotope data indicate that the parental magmas were generated in a post-collisional tectonic setting from a previously subduction-modified mantle source (Wilson et al., 1997).

Although some investigations (Wilson et al., 1997; Tankut et al., 1998) have been carried out, the geochemistry and geochronology of the volcanic rocks of the northwestern part of this province have not been studied in detail. Therefore, discussion of the Miocene volcanism in the GVP still is ongoing due to a lack of systematic geochemical data including whole-rock major oxide and Sr—Nd isotopic and geochronological data (Fourquin et al., 1970; Yihunie, 1993; Wilson et al., 1997). This study focuses on the northwestern part of the GVP, in the Bolu-Ilgaz-Ayaş triangle (Fig. 1) and presents the first $^{40}Ar/^{39}Ar$ age data and new bulk-rock major-trace element, Sr—Nd isotope data and geological mapping of a 100-km^2 area within the northwestern part of the GVP, to

* Corresponding author.
E-mail address: ozdamarse@itu.edu.tr (Ş. Özdamar).

https://doi.org/10.1016/j.jvolgeores.2024.108086
Received 11 October 2023; Received in revised form 16 April 2024; Accepted 25 April 2024
Available online 26 April 2024

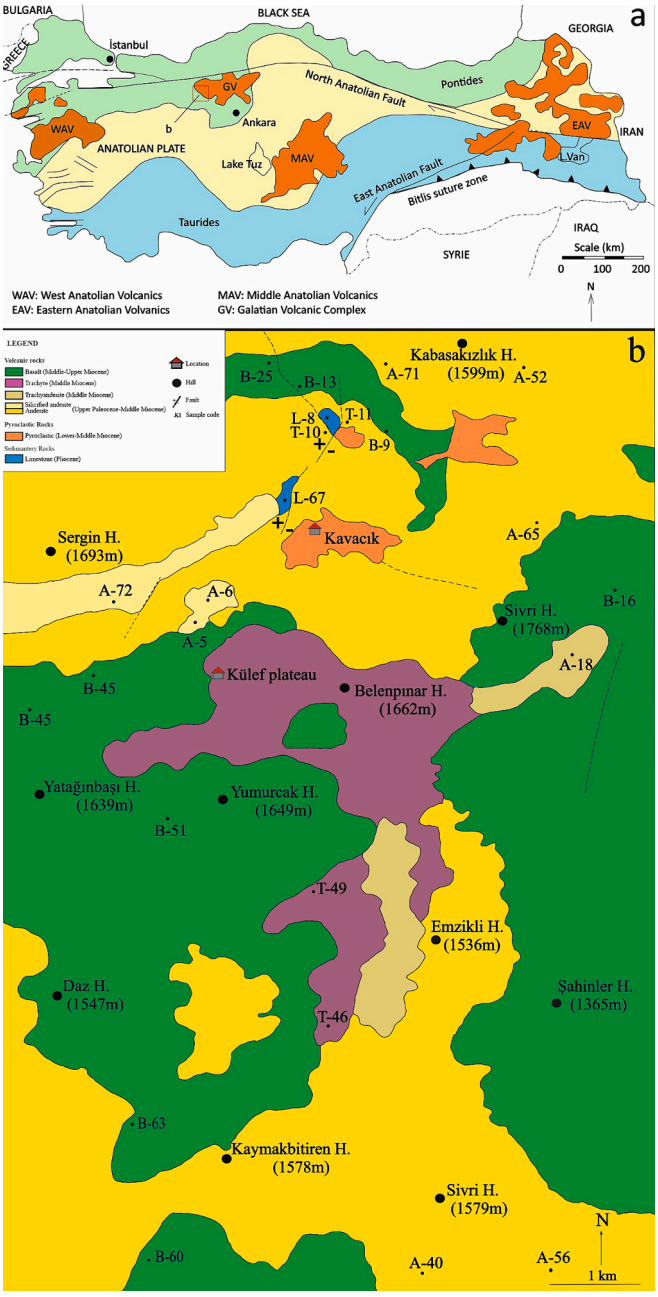

Fig. 1. The geological map of the study area.

investigate the petrogenesis of the Miocene volcanism (Fig. 1). Also, these more reliable $^{40}Ar/^{39}Ar$ age results may contribute to better understand the geodynamic evolution of the GVP.

2. Geological background

The GVP comprises Mesozoic and Tertiary-aged units on a basement consisting of Paleozoic-aged metamorphic units that consist of gneisses and overlying schists of different metamorphism degrees with local marble layers intercalated between them (Toprak et al., 1996). The Mesozoic units unconformable overly the basement rocks and consist of Jurassic to Cretaceous-aged limestones and marls. A red colored-continental Paleocene detrital series, comprising conglomerate, sandstone and clays are deposited in the depressions formed during the Laramian orogenic phase. Eocene marine sediments consisting of conglomeratic sandstones, clays and limestones overlay these detrital series. Upper Paleocene-Upper Miocene volcanics (pyroclastics and lavas) are andesitic, basaltic and trachytic in composition. Upper Paleocene-Lower Eocene aged volcanics cut the Jurassic-Lower Cretaceous sedimentary units. Lower-Middle Miocene aged pyroclastic and volcanic rocks related with lacustrine deposits are unconformable over Mesozoic units. Early-Middle Miocene lavas, pyroclastics and alkali basalts are the main products of the Galatia volcanic complex (Tankut et al., 1998). According to Türkecan (1991), Neogene volcanism with various ages and different chemical compositions was extremely intense in the Köroğlu Volcanic Massif between Bolu-Ankara-Çankırı. Calcalkaline volcanism started in the Lower Miocene and the first products are known as the "Karasivri Volcanites" and consists of dacitic and rhyolitic lavas, tuffs and agglomerates; the "Kirazdağı Volcanites" consists of andesitic and dacitic lavas, tuffs and agglomerates. On these volcanic units, basaltic andesite and andesite Ilıcadere Volcanics, Deveören and Bakacaktepe Volcanics, containing andesitic and dacitic rocks, are located. Upper Miocene lacustrine deposits and basaltic units unconformable overlie these volcanic units (Türkecan, 1991).

3. Local geology and petrography

The study area covers an approximately 100 km^2. It hosts basalt, basaltic andesite, andesite, andesitic basalt, trachy-andesite, basaltic andesite and trachyte lavas, and their pyroclastic equivalents, and limestone (Şahinci, 1975; Tankut et al., 1998; Fig. 1). The volcanic rocks are greyish black, brown, yellowish and green in color and show a porphyritic-aphanitic texture. The basalts widely outcrop around Kavacık village and are black, dark brown and gray in color (Fig. 2a). They are generally massive, rarely in the form of hexagonal cooling columns. Basalts are rarely gas-filled filled with secondary epidote, carbonate and chlorite. Andesites are mainly lavas and outcrop for roughly 50 km^2 around the Akbaş and Makamlar areas in the north of the study area of, mostly in the form of hills and ridges in the north and south of the region. They are black, gray and red in color and mostly show massive character (Fig. 2b, c). Macroscopically, they are coarse-grained, with abundant plagioclase contents that can reach 1–2 mm grain sizes and contains gas cavities. They have enclave that reflect more basic rock fragments. Trachytes and trachy-andesites exposed in the central parts of the study area are mostly fine-grained volcanic and subvolcanic rocks. They are massive, rarely gas-filled, and looks less altered rocks (Fig. 2c, d). The pyroclastic rocks have restricted outcrops are classified as lithic tuff, lapilli tuff, and rarely agglomerate; the tuffs appear light gray in color (Fig. 2e) and comprise lava blocks, limestone pebbles and blocks, agglomerated clasts, pyroxene and plagioclase crystals. The agglomerates comprise basaltic, andesitic and trachytic blocks. Lithostratigraphically, these units are unconformable overlied by Pliocene limestones (Fig. 2f) and Quaternary alluvium (Toori, 2005).

The basalts, andesites, and trachytes have similar petrographic features, having porphyritic textures with moderate phenocrysts contents of about 25–30 vol% (Fig. 3a-g). The basalts display intergranular, porphyritic and ophitic texture (Fig. 3a-c). They comprise plagioclase (labradorite; 40–60 vol%) and clinopyroxene (augite; 35–55 vol%), lesser amounts of amphibole (hornblende) and olivine, and traces of ilmenite, magnetite, sphene. Plagioclase is generally present as microliths and coarse-grained with 0.1–1 mm phenocrysts. Augites are generally coarse-grained components up to 0.4 mm. Hornblende with opacite rims represents the main phenocryst assemblage (Fig. 3b). Rarely observed olivines have a small amount of iddingsite (Fig. 3c). Basaltic andesite and trachy-basalts display hyalo-microlitic porphyritic texture. Phenocrysts occupy ~45 vol% of the total area and consist of mainly plagioclase, pyroxene, amphibole and opaque minerals. They appear in a glassy to microlitic groundmass of plagioclase and pyroxene microlites. The andesites mostly consist of glassy to microlithic matrix with typical porphyritic texture (Fig. 3d-f). They contain mainly plagioclase (30–60 vol%), K-feldspar (<5 vol%) and amphibole (hornblende; 8–20 vol%), biotite (<5 vol%), opaque minerals (magnetite; <2

Fig. 2. Field photos of the studied volcanic rocks (a: basalt, b: andesite, c: trachy-andesite, d: trachyte, e: pyroclastic, f: limestone):

vol%), apatite (<1 vol%), epidote (<2 vol%) and chlorite (<2 vol%). Plagioclases are both phenocrysts with up to 2–3 mm and microliths. They show polysynthetic twinning and locally zoned textures. Volcanic glassy groundmass content of the rock range in between 20 and 30 vol%. Amphiboles are hornblende and generally idiomorphic to hypidiomorphic crystals with grain sizes of 0.8 mm and less are mostly found dispersed in the matrix. Trachytes are distinguished from andesites by higher alkali feldspar and lower plagioclase contents, a fine-grained texture, and the appearance of flow structures (Fig. 3g). The alteration is characterized by secondary carbonate, chlorite, epidote, sericite and clay minerals. Sericitization, argillization and silicification of plagioclases and chloritization of biotites and hornblendes commonly appear. Pyroclastic rocks have undergone hydrothermal alteration and their primary textures have changed (Fig. 3h). Volcanic glassy fragments in the trachytes form the main matrix of the rock samples, and there are quartz, feldspar and minor mica (muscovite) mineral grains and rock fragments, up to 4 mm in size (Fig. 3g). The limestones have micritic, partially oolitic, partially recrystallized texture and are mainly composed of calcite mineral (95–100 vol%), and rare quartz and opaque minerals. The micritic limestones contain fossil and aragonite shells.

4. Analytical methods

A total of 100 samples were collected during a number of field trips. After examination of the samples under Leica polarized-petrography microscope, fresh and representative samples of the study area were selected for bulk-rock major oxide, trace element analysis (22 samples), Sr—Nd isotope geochemistry (4 samples) and Ar/Ar geochronology (2 samples).

The bulk-rock geochemical analyses were performed at Geochemistry Research Laboratories of Istanbul Technical University. To prevent contamination during grinding, all samples were ground to a fine powder at 200 mesh in an agate mortar. The weight loss after lighting a sample split allowed us to calculate the loss on ignition (LOI; at 1050 °C and 12 h). A Bruker S8 Tiger model X-ray fluorescence spectrometer (XRF) with a wavelength range of 0.01–12 nm was used to examine the samples' major oxides, while an ELAN Dynamic Reaction Cell-e (ELAN DRC–e) Perkin Elmer model was used to analyze the samples' trace elements. Two steps were required to completely digest 50 mg of the powdered material. 6 ml of 37% HCl, 2 ml of 65% HNO_3, and 1 ml of 38–40% HF were combined in a pressure– and temperature–controlled Teflon beaker using a Berghoff Microwave at 135 °C to complete the first step. With the addition of 6 ml of 5% boric acid solution, the second stage was finished.

Sr isotope compositions determined at the Radiogenic Isotope Laboratory at Auburn University used a Finnigan MAT 262 thermal ionization mass spectrometer. Eight Faraday cups and a secondary electron multiplier are included in the MAT 262. Using diluted (0.25 N) HNO_3, purified Sr separates are removed from Teflon beakers and combined with a 1 μl TAPH solution (Zou et al., 2000). The combination is then placed as ionization filaments onto degassed rhenium filaments. At 0.7 A (A), Sr samples on single, thin Re filaments are dried. After all of the H_3PO_4 has evaporated, the filament current is gradually increased to 2.0 A, and then it is flushed for a very brief period of time at 3.0 A. Then, a sample magazine with a capacity for up to 13 samples is mounted on filaments containing Sr samples. The magazine is loaded onto the MAT-262 ion source. The vacuum inside the mass spectrometer's ion source and mass analyzer is kept below 10–7 Torr. By running an electric current through the filaments in the ion source, purified Sr samples are thermally ionized. Sr^{+} ions are moved quickly from the ion source into the magnetic sector mass analyzer using an accelerating voltage of 10 KV. For Sr isotope studies, dynamic jumping mode is employed. The ratio of $^{86}Sr/^{88}Sr$ used to standardize Sr isotope compositions is 0.1194. For NIST 987, the measured $^{87}Sr/^{86}Sr$ values are 0.7102510.000011 (*n*

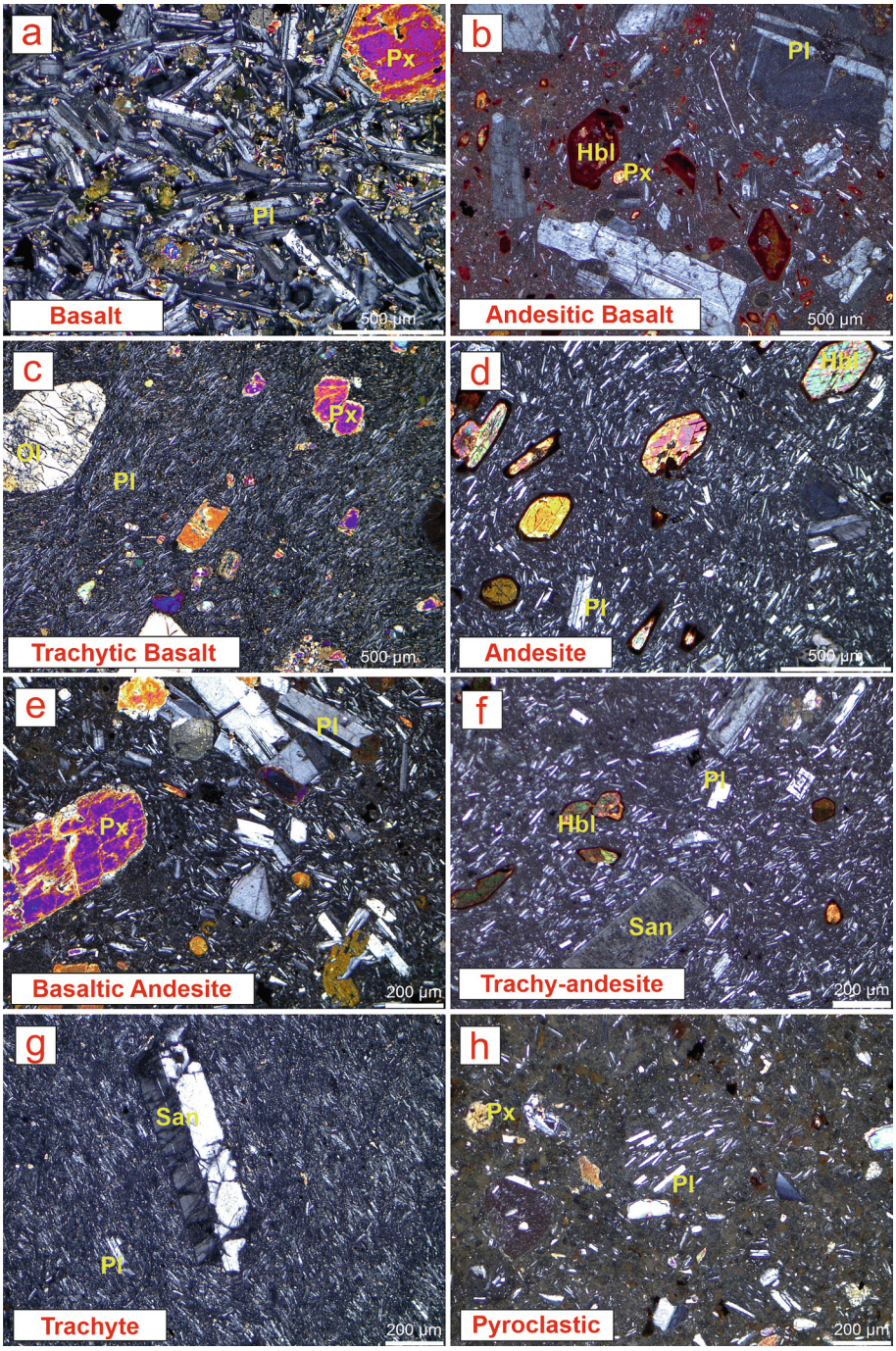

Fig. 3. Photomicrographs showing petrographic characteristics in cross-polarized light of the studied volcanic rocks (a-c: basalt with porphyritic and trachytic texture and iron oxides; d-f: andesite showing hyalo-porphyritic texture and euhedral to subhedral plagioclase and sanidine crystals, and iron oxidized grains; g: trachyte showing flow structure and sanidine grain; h: pyroclastic rocks).

= 12). Rock powders for Nd isotope analyses were dissolved in mixed HNO_3 and HF acids. After chromatography column chemistry, purified Nd separates were analyzed by a Neptune Plus MC-ICP-MS (Thermo Fisher Scientific, Dreieich, Germany) at the Wuhan Sample Solution Analytical Technology. Measured $^{143}Nd/^{144}Nd$ values for JNdi-1 standard, BCR-2, and RGM-2 are 0.512116 ± 0.000011 (2SD, n = 7), 0.512646 ± 0.000007, and 0.512809 ± 0.000010, respectively, identical within uncertainties to their published values (Li et al., 2012; Tanaka et al., 2000).

To constrain the age span of lavas, the samples (T6 and A71) were crushed, sieved and cleaned using alternate de-ionized water and ethanol and packaged in aluminium foil packets of ca. 10 mm × 10 mm in size prior to irradiation. Samples were irradiated at the McMaster Nuclear Reactor (McMaster University, Canada) for 83 h. Cadmium shielding was used and the samples were held in position 8D. Irradiated samples were analyzed in the Ar/Ar and Noble Gas Research Laboratory Faculty of STEM at the Open University. The biotite mineral standard GA1550, which has an age of 99.738 0.104 Ma, was used to measure the neutron flux (Renne et al., 2011). The unknown samples were packed either side of standards for irradiation, and the standards were then analyzed utilizing the single grain fusion technique using a 1059 nm CSI fiber laser and a MAP215–50 mass spectrometer. A 1% error on J is utilized, and the J Values were then estimated by linear extrapolation between the two recorded J Values. The values for each sample are

Table 1
Ar/Ar geochronology results of the samples.

	Step	^{40}Ar	+/−	^{39}Ar	+/−	^{38}Ar	+/−	^{37}Ar	+/−	^{36}Ar	+/−	^{40}Ar*/^{39}Ar	+/−	Age	+/−	39/40	+/−	36/40	+/−	37/39	+/−	38/39	+/−
	1	0,01194	0,00053	0,00535	0,00017	0,00007	0,00003	0,00323	0,00023	−0,00002	0,00002	32,130	10,112	45,56	27,86	0,4482	0,0242	0,0015	−0,0015	0,6040	0,0469	0,0127	0,0065
	2	0,06901	0,00233	0,01906	0,00073	0,00028	0,00006	0,01132	0,00023	0,00014	0,00002	14,267	0,4131	20,38	11,26	0,2762	0,0141	0,0020	0,0004	0,5941	0,0257	0,0146	0,0033
	3	0,33,674	0,00221	0,06212	0,00129	0,00103	0,00004	0,03685	0,00023	0,00075	0,00003	18,032	0,1693	25,74	4,67	0,1845	0,0040	0,0022	0,0001	0,5931	0,0129	0,0166	0,0008
	4	0,86,941	0,00299	0,17,565	0,00065	0,00271	0,00013	0,08777	0,00016	0,00203	0,00008	14,969	0,1403	21,40	3,89	0,2020	0,0010	0,0023	0,0001	0,4997	0,0021	0,0154	0,0008
	5	272,427	0,00759	0,35,569	0,00456	0,00637	0,00022	0,15,779	0,00016	0,00726	0,00020	15,643	0,1711	22,35	4,75	0,1306	0,0017	0,0027	0,0001	0,4436	0,0057	0,0179	0,0007
	6	308,048	0,00771	0,45,598	0,00174	0,00765	0,00039	0,22,174	0,00016	0,00786	0,00011	16,076	0,0754	22,97	2,07	0,1480	0,0007	0,0026	0,0000	0,4863	0,0019	0,0168	0,0009
	7	106,477	0,00655	0,21,443	0,00188	0,00313	0,00014	0,13,134	0,00016	0,00255	0,00008	14,169	0,1189	20,24	3,27	0,2014	0,0022	0,0024	0,0001	0,6125	0,0054	0,0146	0,0007
Sample 6	8	193,712	0,00607	0,38,302	0,00179	0,00601	0,00016	0,22,516	0,00016	0,00444	0,00009	15,953	0,0740	22,78	2,04	0,1977	0,0011	0,0023	0,0000	0,5879	0,0028	0,0157	0,0004
	9	131,157	0,00751	0,21,831	0,00109	0,00371	0,00020	0,13,732	0,00016	0,00326	0,00007	15,536	0,1050	22,20	2,86	0,1664	0,0013	0,0025	0,0001	0,6290	0,0032	0,0170	0,0009
	10	150,069	0,01138	0,32,683	0,00186	0,00518	0,00008	0,23,860	0,00016	0,00322	0,00008	16,522	0,0836	23,59	2,23	0,2178	0,0021	0,0021	0,0001	0,7300	0,0042	0,0159	0,0003
	11	111,454	0,00372	0,29,771	0,00048	0,00430	0,00013	0,24,567	0,00016	0,00243	0,00007	13,110	0,0742	18,75	2,06	0,2671	0,0010	0,0022	0,0001	0,8252	0,0014	0,0144	0,0004
	12	0,69,308	0,00288	0,12,728	0,00057	0,00187	0,00015	0,09947	0,00016	0,00163	0,00007	16,267	0,1710	23,23	4,76	0,1836	0,0011	0,0023	0,0001	0,7815	0,0038	0,0147	0,0012
	13	124,092	0,00323	0,28,512	0,00189	0,00423	0,00023	0,24,651	0,00016	0,00284	0,00012	13,832	0,1283	19,77	3,57	0,2298	0,0016	0,0023	0,0001	0,8646	0,0058	0,0148	0,0008
	14	0,98,408	0,00636	0,26,185	0,00135	0,00377	0,00015	0,26,944	0,00018	0,00181	0,00007	16,937	0,0874	24,18	2,38	0,2661	0,0022	0,0018	0,0001	10,290	0,0054	0,0144	0,0006
	15	143,468	0,00324	0,29,797	0,00135	0,00470	0,00015	0,27,084	0,00018	0,00326	0,00007	15,482	0,0745	22,12	2,06	0,2077	0,0011	0,0023	0,0001	0,9089	0,0042	0,0158	0,0005
	1	0,02928	0,00081	0,01415	0,00059	0,00008	0,00004	0,00629	0,00018	0,00005	0,00003	10,865	0,5629	15,50	15,64	0,4833	0,0243	0,0016	0,0009	0,4447	0,0226	0,0058	0,0030
	2	0,22,680	0,00142	0,08808	0,00060	0,00121	0,00009	0,04190	0,00018	0,00032	0,00003	15,027	0,1191	21,40	3,29	0,3884	0,0036	0,0014	0,0002	0,4757	0,0038	0,0137	0,0010
	3	0,36,388	0,00390	0,17,255	0,00178	0,00232	0,00009	0,06938	0,00018	0,00037	0,00003	14,715	0,0661	20,96	1,79	0,4742	0,0070	0,0010	0,0001	0,4021	0,0043	0,0135	0,0005
	4	0,48,118	0,00109	0,23,717	0,00103	0,00331	0,00014	0,10,799	0,00018	0,00039	0,00004	15,414	0,0448	21,95	1,24	0,4929	0,0024	0,0008	0,0001	0,4553	0,0021	0,0139	0,0006
	5	0,34,694	0,00205	0,17,977	0,00131	0,00231	0,00013	0,09076	0,00018	0,00025	0,00003	15,111	0,0472	21,52	1,30	0,5182	0,0049	0,0007	0,0001	0,5048	0,0038	0,0129	0,0008
Sample 71	6	0,26,452	0,00109	0,14,814	0,00111	0,00196	0,00016	0,09209	0,00018	0,00019	0,00003	13,991	0,0555	19,93	1,53	0,5600	0,0048	0,0007	0,0001	0,6216	0,0048	0,0132	0,0011
	7	0,46,518	0,00175	0,23,440	0,00149	0,00310	0,00021	0,16,663	0,00018	0,00040	0,00004	14,748	0,0577	21,01	1,60	0,5039	0,0037	0,0009	0,0001	0,7109	0,0046	0,0132	0,0009
	8	0,25,728	0,00248	0,15,468	0,00155	0,00200	0,00010	0,11,292	0,00037	0,00017	0,00004	13,363	0,0819	19,05	2,27	0,6012	0,0084	0,0007	0,0002	0,7300	0,0077	0,0130	0,0006
	9	0,17,856	0,00194	0,09515	0,00102	0,00126	0,00005	0,08935	0,00037	0,00016	0,00003	13,864	0,1011	19,75	2,79	0,5329	0,0081	0,0009	0,0002	0,9390	0,0108	0,0132	0,0006
	10	0,17,937	0,00122	0,08785	0,00079	0,00120	0,00008	0,09640	0,00037	0,00015	0,00002	15,178	0,0767	21,62	2,12	0,4898	0,0055	0,0009	0,0001	10,973	0,0107	0,0137	0,0009
	11	0,18,950	0,00140	0,11,687	0,00063	0,00137	0,00013	0,10,394	0,00037	0,00007	0,00002	14,376	0,0578	20,48	1,60	0,6167	0,0056	0,0004	0,0001	0,8893	0,0058	0,0117	0,0011
	12	0,13,728	0,00375	0,05676	0,00158	0,00071	0,00008	0,08311	0,00037	0,00012	0,00003	17,978	0,1837	25,57	4,95	0,4135	0,0161	0,0009	0,0002	14,641	0,0412	0,0125	0,0014

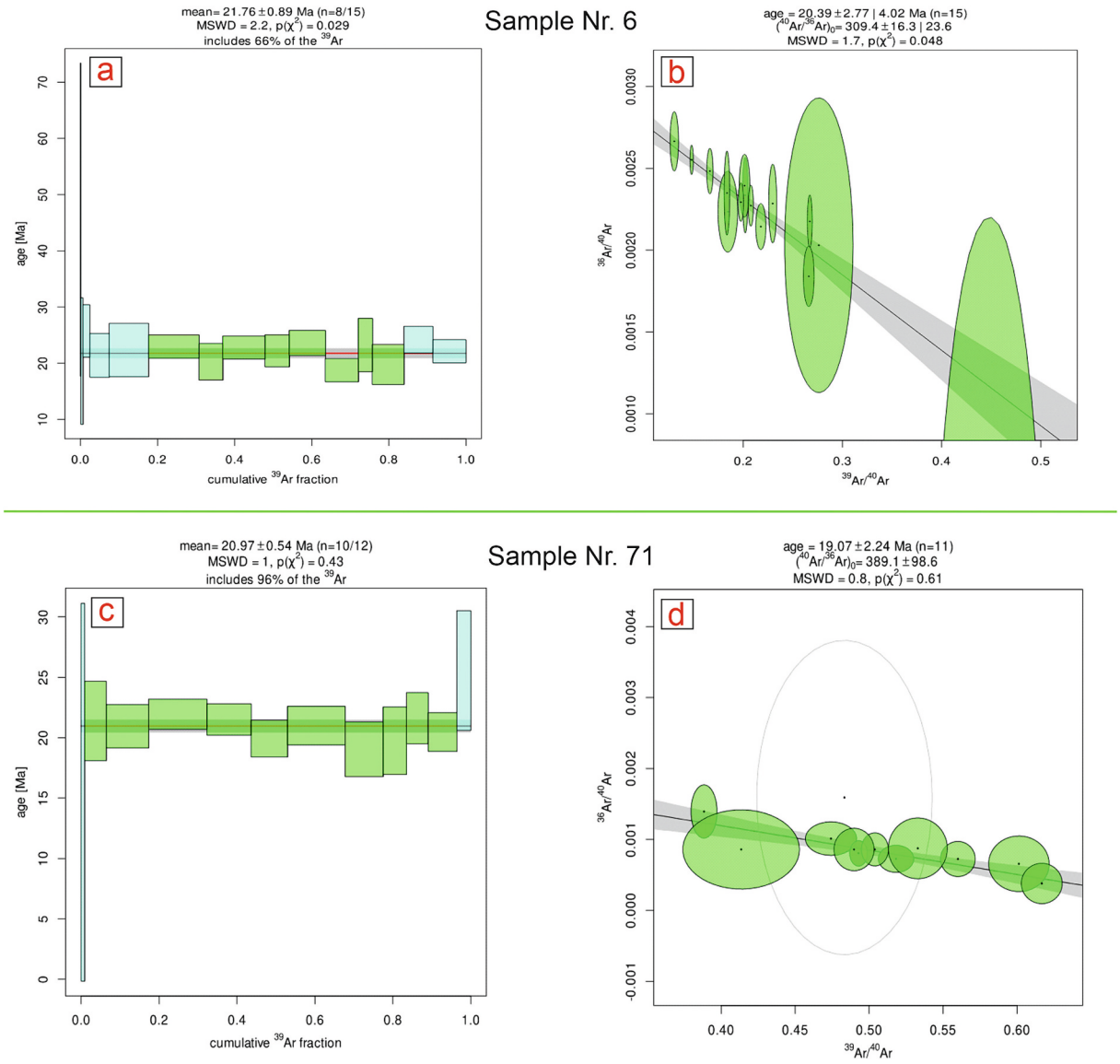

Fig. 4. (a) Whole-rock T6 step-heating release spectra, (b) whole-rock T6 inverse isochron correlation plot, (c) whole-rock A71 step-heating release spectra and (d) whole-rock A71 inverse isochron correlation plot (blue steps not included in the calculation). (For interpretation of the references to color in this figure legend, the reader is referred to the web version of this article.)

displayed in the attached spreadsheet. The irradiated samples were fed into an ultra-high vacuum system, where a 1059 nm CSI fiber laser was used to step-heat the two basalt separates and the feldspar separate, fuse individual grains of the other mineral separates (biotite and hornblende), and irradiate the samples. A MAP 215–50 mass spectrometer was used to measure the extracted gases' mass discrimination value, which was determined to be 1.005005 from ^{40}Ar (using a calibration noble gas mixture of known composition), after being cleaned for 5 min with two SAES AP-10 getters operating at 450 °C and room temperature, respectively. System blanks were measured prior to and following each sample analysis of one to two. The measurement of ^{40}Ar, ^{39}Ar, ^{38}Ar, ^{37}Ar, and ^{36}Ar, each for 10 scans, is part of the fully automated gas clean-up and inlet process. The final readings are extrapolations back to the inlet time. The system blanks were deducted from the raw sample data before and after every one or two sample analyses. Results were adjusted to account for the nuclear reactor's neutron-induced interference processes as well as ^{37}Ar and ^{39}Ar decay. Based on investigations of Ca and K salts, the correction factors (^{39}Ar/^{37}Ar)Ca = 0.000720.000014, (^{36}Ar/^{37}Ar)Ca = 0.00028880.000047, and (^{40}Ar/^{39}Ar)K = 0.002290.00031 were applied. The atmospheric ^{40}Ar/^{36}Ar ratio of 298.56 0.31 (Lee et al., 2006) and the decay constants of Renne et al. (2011) were used to compute ages. Ages were calculated using IsoplotR (Vermeesch, 2018), with all ages presented at the 2 level and with a 1% error on the J value. All data adjustments were performed using an Excel macro. The 'plateau age' according to Isoplot R is the weighted mean age of the longest chain of succeeding steps that satisfy a modified Chauvenet criterion and have a cumulative ^{39}Ar content of less than or equal to 0. Data for ^{40}Ar/^{39}Ar are shown in Table 1.

5. Geochronological results

To constrain the timing of volcanism in the GVP, we selected two the freshest and representative samples (T6 and A71) from trachytes and andesites, respectively) for ^{40}Ar/^{39}Ar dating by step-heating analysis. For whole-rock sample T6, the step heating results produce a plateau age of 21.76 ± 0.89 Ma (Fig. 4a), and an inverse isochron age of 20.39 ± 2.77 Ma (Fig. 4b), within error of one another and with an ^{40}Ar/^{36}Ar intercept within error of atmospheric at 309.4 ± 16.3 (atmospheric ratio of 298.56, Lee et al., 2006). Sample A71 produced a plateau age of 20.97 ± 0.54 Ma (Fig. 4c) and an inverse isochron age of 19.08 ± 2.24 Ma

Table 2
Major oxides (wt%) compositions of the Bolu volcanics.

Sample	A-9	A-10	A-11	A-45	A-51	A-60	A-63	A-65	A-71	B-13	B-16	B-25	B-44	B-49	T-5	T-6	T-18	T-40	T-46	T-52	T-56	T-72
Major Oxides (%wt.)																						
SiO_2	57,90	55,90	61,30	50,10	49,10	56,50	52,20	50,90	54,80	50,40	47,50	48,60	48,30	48,80	64,80	65,40	67,20	62,10	63,70	63,40	66,30	66,50
Al_2O_3	19,05	19,50	18,65	17,55	17,05	18,15	16,70	18,15	20,40	18,25	15,70	15,90	17,00	17,00	16,10	16,55	17,20	17,40	17,70	19,00	17,65	16,55
Fe_2O_3	5,12	4,90	5,03	7,23	7,09	6,38	7,95	5,54	6,97	8,06	8,60	9,01	7,79	7,16	3,58	3,85	3,34	4,87	3,91	3,32	3,28	3,75
MgO	1,55	1,15	0,71	6,80	6,68	1,49	4,29	1,59	1,80	4,94	10,05	9,44	7,28	6,79	1,31	0,48	0,24	0,89	0,51	0,29	0,27	1,02
CaO	4,84	5,49	4,61	8,81	2,05	6,03	8,98	4,86	7,28	7,91	8,52	8,76	9,64	9,14	3,68	3,26	2,78	3,90	3,38	3,06	2,02	3,69
Na_2O	4,59	2,98	5,05	4,32	4,04	4,60	4,48	4,48	5,26	4,05	3,60	3,61	3,55	3,81	3,82	4,33	4,58	4,84	4,16	5,44	4,79	4,27
K_2O	1,93	0,87	2,16	2,55	2,37	2,21	1,24	2,40	1,72	1,30	1,72	1,97	2,25	2,21	2,88	2,59	3,13	3,14	2,80	2,64	3,75	2,63
TiO_2	0,08	1,06	0,69	1,41	1,40	1,09	1,18	0,68	1,15	1,28	1,42	1,46	1,42	1,43	0,59	0,64	0,59	0,78	0,72	0,51	0,51	0,62
P_2O_5	0,37	0,16	0,38	0,71	0,71	0,46	0,86	0,37	0,53	0,41	0,55	0,51	0,72	0,70	0,21	0,17	0,18	0,32	0,20	0,28	0,12	0,21
MnO	0,06	0,08	0,04	0,12	0,12	0,05	0,13	0,06	0,09	1,28	1,42	0,14	0,13	0,12	0,12	0,03	0,06	0,07	0,03	0,07	0,05	0,05
Cr_2O_3	0,01	0,01	0,01	0,02	0,03	0,01	0,03	0,01	0,00	0,01	0,06	0,07	0,02	0,03	0,01	0,00	0,00	0,01	<0.002	0,00	0,00	0,00
SrO	0,07	0,05	0,09	0,10	0,09	0,06	0,08	0,06	0,09	0,07	0,06	0,08	0,12	0,10	0,02	0,01	0,01	0,07	0,03	0,06	0,03	0,03
BaO	0,05	0,09	0,07	0,07	0,07	0,05	0,08	0,06	0,09	0,03	0,07	0,07	0,08	0,07	0,06	0,05	0,07	0,07	0,06	0,05	0,08	0,07
LOI	2,91	8,71	2,50	1,34	2,36	3,40	1,66	2,96	1,33	2,47	1,73	1,62	2,32	2,19	1,34	2,31	1,68	2,34	2,54	2,24	1,89	1,80
Total	99,28	100,95	101,29	101,13	100,11	100,48	99,86	101,12	101,51	99,31	99,72	101,24	100,80	99,55	98,52	99,67	101,06	100,80	99,74	100,36	100,74	101,19

(Table 1 and Fig. 4d). These 2 ages are within error of each other and the $^{40}Ar/^{36}Ar$ intercept on the isochron is within error of the atmospheric ratio (388.1 ± 98.1), but this may be due to the larger error on the isochron.

6. Whole-rock major and trace element geochemistry

Based on petrographic observations and LOI, the GVP samples under study have generally undergone weak to moderate alteration; we consider the impact of these events by highlighting the transition elements, REEs, and HFSEs, as well as Th and Ti in mafic rocks, which are relatively stable during alteration (Staudigel et al., 1995). Tables 2 and 3 give the major oxide and trace element values of 22 representative samples of andesite, trachyte, and basalt from the GVP. In the total alkalies versus silica (TAS) diagram of Le Bas et al. (1986) was used to classify the volcanic rocks, the samples plot in the trachy-basalt, basaltic trachy-andesite, trachy-andesite, andesite, trachy-dacite and dacite fields consistent with the mineralogy and petrography (Fig. 5a) (all plots are on anhydrous basis). All samples show calc-alkaline affinity on the AFM diagram (Fig. 5b) and indicate calc-alkaline and shoshonitic/high-K calcalkaline character (Fig. 5c).

The intermediate compositions are dominant in all analyzed samples. The data reveals that the complete volcanic rocks is a continuous mafic-intermediate magma suite, with a large compositional range and no chemical compositional break. Loss on ignition (LOI) values are <2 wt% except for some samples. SiO_2 contents vary between 50.9 wt% and 67.2 wt%. The high SiO_2 range of silicified trachyte (T5; 67.2 wt%) is consistent with the petrographic observations (mineralogical compositions and phenocryst/matrix ratio etc.). Andesite and basalt samples have higher CaO contents than trachyte with 4.61 to 9.64 wt. percentage. The total alkalies ($Na_2O + K_2O$) contents of all samples vary between 6.88 wt% and 8.10 wt%.

The variations of all major oxides with increasing SiO_2 in the GVP samples are given in Fig. 6. Al_2O_3, Na_2O and K_2O show positive trends and/or no good correlations, whereas CaO, MgO, TiO_2, P_2O_5 and FeO_T show negative good correlations with SiO_2, consistent with derivation of the more silica-rich magmas by crystal fractionation from a more mafic parent magma. REE contents display a descending pattern towards the heavy REE. REE values for all samples are variable, for andesites and trachytes, while for basalt is more homogeneous (Fig. 7a, b). They display enrcihment of Cs, Rb, Ba, Th, U and Pb while depletion K and Ti, which are signitures of arc-related magmatic rocks (Pearce and Parkinson, 1993) and are quite common in *syn*- to postcollisional rocks (Pearce et al., 1984). Negligible Eu anomalies lead us to exclude any relevant role for amphibole and plagioclase fractionation.

7. Whole-rock Sr and Nd isotope geochemistry

Four samples (T6, A9, A71 and T72) from the GVP were analyzed for their whole-rock Sr—Nd isotopic compositions and the results are given in Table 4. The initial Sr and Nd values were calculated at an age of 21.36 ± 0.71, an average plateau ages of the T6 and A71 samples. They display relatively homogeneous initial isotopic compositions of $^{87}Sr/^{86}Sr$ ranging from 0.704619 and 0.704998 and $^{143}Nd/^{144}Nd$ ratios from 0.512673 and 0.512755, suggesting no effect on Nd and Sr isotopic ratios by alteration. Fig. 8 show that the samples have higher (Sr/Sr) and lower (Nd/ Nd) ratios than any of the Kula volcanics and have similar isotopic ratios with Western Anatolia Oligocene to Miocene granites.

8. Discussion

The petrogenesis, tectonic setting and timing of the volcanism can be discussed in terms of their whole-rock major and trace element compositions, Sr and Nd isotopic and age data.

Table 3
Trace elements (ppm) and rare earth elements (ppm) compositions of the Bolu volcanics.

Sample	A – 9	A – 10	A – 11	A – 45	A – 51	A – 60	A – 63	A – 65	A – 71	B – 13	B – 16	B – 25	B – 44	B – 49	T – 5	T – 6	T – 18	T – 40	T – 46	T – 52	T – 56	T – 72
Trace Elements (ppm)																						
Au	0,01	–	–	–	0,01	–	–	–	0,01	0,01	0,01	0,01	0,01	–	–	–	–	0,01	–	<0.005	–	0,01
Ag	<0.5	<0.5	<0.5	<0.5	<0.5	<0.5	<0.5	<0.5	<0.5	<0.5	<0.5	<0.5	<0.5	<0.5	1,30	0,50	<0.5	<0.5	<0.5	<0.5	<0.5	<0.5
Al	0,25	9,36	8,77	8,27	8,23	8,69	8,55	8,53	9,13	8,24	7,73	7,92	8,10	8,10	7,87	8,09	8,05	8,41	8,90	9,01	8,64	7,85
As	<5	<5	6,00	<5	<5	<5	<5	<5	<5	<5	<5	7,00	<5	<5	36,00	<5	<5	<5	<5	<5	<5	<5
Ba	500,00	790,00	630,00	640,00	600,00	470,00	780,00	540,00	740,00	290,00	670,00	660,00	750,00	660,00	550,00	430,00	590,00	620,00	540,00	490,00	710,00	580,00
Be	2,30	2,10	2,50	1,50	1,50	2,00	1,80	1,70	2,80	1,40	1,30	1,20	1,40	1,40	1,70	1,90	3,10	2,20	1,60	1,80	2,70	1,60
Bi	<2	2,00	<2	<2	<2	<2	2,00	<2	<2	<2	<2	<2	<2	<2	2,00	<2	2,00	2,00	5,00	<2	<2	<2
Ca	3,43	3,67	3,11	5,87	6,18	4,17	5,94	3,21	4,72	5,40	5,72	5,81	6,30	6,23	2,50	2,26	1,88	2,66	2,27	2,07	1,37	2,41
Cd	<0.5	<0.5	<0.5	<0.5	<0.5	<0.5	<0.5	<0.5	<0.5	<0.5	<0.5	<0.5	<0.5	<0.5	<0.5	<0.5	<0.5	<0.5	<0.5	<0.5	<0.5	<0.5
Co	9,00	20,00	7,00	30,00	27,00	15,00	30,00	12,00	16,00	27,00	43,00	44,00	30,00	27,00	13,00	5,00	6,00	14,00	5,00	6,00	55,00	7,00
Cr	56,00	44,00	32,00	123,00	133,00	64,00	138,00	23,00	11,00	20,00	282,00	320,00	124,00	145,00	17,00	16,00	2,00	57,00	3,00	11,00	2,00	17,00
Cs	1,25	2,02	1,43	0,85	0,87	1,73	57,60	2,43	0,56	0,73	0,60	0,98	1,03	0,68	3,52	2,46	2,78	1,69	2,55	2,11	2,42	2,11
Cu	12,00	13,00	18,00	42,00	39,00	39,00	44,00	17,00	30,00	28,00	47,00	51,00	40,00	39,00	9,00	7,00	8,00	25,00	15,00	13,00	7,00	14,00
Fe	3,53	3,24	3,34	4,91	4,89	4,37	5,31	3,62	4,54	5,38	5,82	6,14	5,26	4,86	2,39	2,62	2,21	3,26	2,54	2,26	2,22	2,42
Ga	20,00	20,00	20,00	20,00	20,00	20,00	20,00	20,00	20,00	20,00	10,00	10,00	20,00	20,00	20,00	20,00	20,00	20,00	20,00	20,00	20,00	20,00
Hf	6,00	5,00	5,20	4,20	4,10	5,60	4,90	5,00	4,60	4,20	3,70	3,60	4,00	4,00	5,30	5,00	6,00	6,20	5,40	5,20	6,80	5,00
K	1,62	0,71	1,75	2,00	1,84	1,76	1,02	1,87	1,28	0,97	1,37	1,56	1,77	1,70	2,42	2,10	2,43	2,45	2,16	2,14	3,00	2,02
Mg	0,84	0,57	0,36	3,88	3,85	0,82	2,38	0,83	0,90	2,72	5,89	5,46	4,04	3,89	0,70	0,25	0,12	0,46	0,26	0,15	0,14	0,52
Mn	426,00	624,00	335,00	907,00	907,00	361,00	967,00	430,00	634,00	968,00	1.020,00	1.040,00	952,00	886,00	903,00	196,00	435,00	508,00	226,00	528,00	398,00	360,00
Mo	1,00	<1	1,00	1,00	<1	1,00	<1	1,00	1,00	2,00	1,00	1,00	1,00	<1	2,00	1,00	1,00	1,00	1,00	<1	3,00	1,00
Na	3,26	2,08	3,42	3,02	3,01	3,22	3,17	3,12	3,58	2,90	2,53	2,53	2,52	2,82	2,68	2,90	3,16	3,36	2,87	3,83	3,36	2,94
Nb	23,90	18,80	21,30	41,50	41,30	31,60	35,10	20,90	22,10	15,70	37,40	35,60	39,20	40,10	16,00	16,10	22,40	32,50	21,20	26,30	33,80	15,60
Ni	45,00	42,00	40,00	110,00	116,00	52,00	98,00	18,00	23,00	30,00	264,00	285,00	96,00	111,00	9,00	13,00	2,00	55,00	6,00	14,00	2,00	19,00
P	1.710,00	730,00	1.590,00	3.230,00	3.120,00	2.330,00	3.640,00	1.610,00	2.320,00	1.890,00	2.500,00	2.470,00	3.230,00	3.130,00	830,00	860,00	870,00	1.620,00	940,00	1.300,00	540,00	950,00
Pb	5,00	5,00	52,00	3,00	2,00	14,00	24,00	20,00	18,00	26,00	4,00	20,00	14,00	5,00	685,00	6,00	16,00	18,00	19,00	13,00	24,00	18,00
Pr	8,28	8,51	8,46	8,83	8,46	10,55	12,85	8,49	9,69	6,70	6,47	6,25	9,29	8,62	6,01	5,65	7,83	12,15	5,49	8,48	9,09	6,34
Rb	43,70	22,40	46,90	44,00	104,00	48,70	15,90	57,30	26,30	26,10	64,50	35,70	41,70	52,00	87,80	81,90	94,00	82,20	77,50	60,50	112,50	84,20
S	0,02	0,01	0,02	0,01	0,01	<0.01	<0.01	0,01	0,02	0,01	<0.01	<0.01	0,01	0,01	0,02	0,01	<0.01	<0.01	<0.01	0,01	<0.01	0,01
Sb	<5	<5	6,00	<5	<5	<5	<5	<5	<5	<5	<5	<5	<5	<5	12,00	<5	<5	<5	<5	<5	<5	<5
Sn	1,00	2,00	1,00	1,00	1,00	2,00	2,00	2,00	1,00	1,00	1,00	1,00	1,00	1,00	3,00	2,00	2,00	1,00	2,00	1,00	2,00	2,00
Sr	839,00	638,00	822,00	1.120,00	1.120,00	793,00	991,00	748,00	1.070,00	752,00	845,00	932,00	1.225,00	1.115,00	398,00	372,00	404,00	648,00	435,00	854,00	468,00	383,00
Ta	1,40	1,00	1,20	2,00	1,90	1,60	1,60	1,20	<20	0,80	1,80	1,60	1,90	1,80	1,10	1,00	20,00	1,90	1,30	1,40	2,00	<20
Ti	0,49	0,62	0,39	0,78	0,80	0,61	0,69	0,39	0,62	0,70	0,80	0,80	0,81	0,80	0,36	0,37	0,32	0,42	0,40	0,29	0,28	0,34
Th	11,35	8,04	9,33	4,66	4,44	12,8	10,9	10,15	6,57	4,34	3,78	3,54	4,42	4,42	9,8	9,81	13,9	17,05	12,65	12,95	21,4	9,75
TI	<10	<10	<10	<10	<10	<10	<10	<10	<10	<10	<10	<10	<10	<10	10,00	<10	<10	<10	<10	<10	<10	<10
U	2,89	1,20	2,95	1,30	1,27	3,27	2,96	2,71	1,68	1,41	1,06	0,98	1,27	1,25	3,08	2,99	3,52	4,67	3,04	3,92	5,89	2,94
V	72,00	58,00	65,00	136,00	138,00	106,00	142,00	73,00	134,00	132,00	134,00	142,00	153,00	143,00	44,00	45,00	34,00	63,00	51,00	52,00	31,00	48,00
W	<10	<10	<10	<10	<10	<10	<10	<10	<10	<10	<10	<10	<10	<10	<10	<10	<10	<10	<10	<10	<10	<10
Zn	66,00	64,00	88,00	79,00	70,00	107,00	104,00	89,00	130,00	92,00	74,00	75,00	80,00	71,00	76,00	54,00	90,00	92,00	65,00	64,00	100,00	68,00
Zr	271,00	219,00	239,00	199,00	192,00	274,00	231,00	235,00	219,00	192,00	171,00	167,00	190,00	189,00	230,00	227,00	273,00	286,00	255,00	266,00	345,00	226,00
Rare Earth Elements (ppm)																						
La	40,00	30,00	40,00	30,00	30,00	40,00	50,00	30,00	30,00	20,00	20,00	20,00	30,00	30,00	30,00	30,00	30,00	50,00	20,00	40,00	40,00	20,00
Ce	72,20	68,80	74,70	76,10	72,60	86,60	110,50	72,90	80,80	55,80	54,60	52,30	79,20	73,70	54,60	50,00	69,20	90,50	50,80	79,80	80,30	55,80
Sc	8,00	9,00	6,00	14,00	15,00	11,00	15,00	6,00	9,00	12,00	17,00	18,00	16,00	16,00	4,00	5,00	2,00	7,00	4,00	4,00	2,00	5,00
Y	14,00	16,80	13,20	18,90	18,80	36,60	24,90	15,90	23,30	22,50	19,70	18,60	19,50	18,80	13,50	12,50	16,50	24,50	9,70	12,50	13,40	16,50
Nd	27,90	29,50	28,40	32,80	31,70	37,90	46,70	29,90	36,00	25,90	25,20	24,30	34,30	32,10	21,20	19,50	25,50	40,10	18,60	28,20	28,10	22,80
Sm	4,49	5,10	4,19	5,23	5,27	6,17	7,27	4,72	6,16	5,11	4,45	4,43	5,74	5,50	3,45	3,32	3,89	6,18	2,82	3,94	3,86	3,81
Eu	1,34	1,47	1,32	1,67	1,60	1,78	2,09	1,25	1,76	1,60	1,64	1,48	1,70	1,66	0,97	1,00	1,05	1,63	1,04	1,11	1,15	1,03
Gd	3,73	4,41	3,42	4,71	4,52	5,89	5,75	3,65	5,33	4,72	4,43	4,34	4,62	4,58	2,98	2,86	3,18	5,29	2,40	2,92	2,62	3,36
Tb	0,50	0,60	0,44	0,63	0,64	0,84	0,82	0,50	0,75	0,67	0,65	0,62	0,67	0,65	0,42	0,40	0,43	0,76	0,32	0,41	0,41	0,47

(*continued on next page*)

Table 3 (*continued*)

Sample	A-9	A-10	A-11	A-45	A-51	A-60	A-63	A-65	A-71	B-13	B-16	B-25	B-44	B-49	T-5	T-6	T-18	T-40	T-46	T-52	T-56	T-72
Dy	2,90	3,66	2,61	3,84	3,87	5,70	4,85	3,19	4,45	4,43	4,03	3,76	3,97	3,80	2,55	2,54	2,67	4,49	1,93	2,31	2,32	2,99
Ho	0,54	0,69	0,47	0,77	0,73	1,17	0,94	0,59	0,89	0,89	0,79	0,78	0,78	0,75	0,52	0,47	0,52	0,86	0,36	0,44	0,51	0,56
Er	1,48	1,75	1,42	1,96	2,10	3,48	2,52	1,56	2,53	2,45	2,05	2,09	1,93	2,00	1,38	1,28	1,49	2,49	1,07	1,23	1,40	1,63
Tm	0,20	0,24	0,19	0,27	0,25	0,49	0,35	0,24	0,32	0,37	0,27	0,28	0,28	0,28	0,21	0,19	0,20	0,38	0,14	0,18	0,19	0,21
Yb	1,40	1,59	1,25	1,82	1,78	3,27	2,27	1,68	2,36	2,19	1,92	1,80	1,77	1,77	1,42	1,26	1,35	2,32	0,94	1,25	1,36	1,46
Lu	0,21	0,24	0,18	0,29	0,26	0,55	0,35	0,23	0,35	0,35	0,29	0,29	0,28	0,27	0,21	0,20	0,22	0,38	0,15	0,21	0,23	0,22
REE	178,89	173,85	177,79	192,99	189,12	241,44	274,31	172,31	204,00	158,98	157,02	153,07	200,74	191,86	137,41	130,52	158,20	236,88	114,27	178,50	177,85	135,84
Eu/Eu*	0,97	0,93	1,04	1,01	0,98	0,89	0,96	0,89	0,92	0,98	1,12	1,02	0,98	0,98	0,90	0,97	0,89	0,85	1,19	0,96	1,05	0,86
$(La/Yb)_N$	19,31	12,75	21,62	11,14	11,39	8,27	14,88	12,07	8,59	6,17	7,04	7,51	11,45	11,45	14,28	16,09	15,02	14,56	14,38	21,62	19,87	9,26
Na_2O/K_2O	2,38	3,43	2,34	1,69	1,70	2,08	3,61	1,87	3,06	3,12	2,09	1,83	1,58	1,72	1,33	1,67	1,46	1,54	1,49	2,06	1,28	1,62
K_2O/Na_2O	0,42	0,29	0,43	0,59	0,59	0,48	0,28	0,54	0,33	0,32	0,48	0,55	0,63	0,58	0,75	0,60	0,68	0,65	0,67	0,49	0,78	0,62
$Na_2O + K_2O$	6,52	3,85	7,21	6,87	6,41	6,81	5,72	6,88	6,98	5,35	5,32	5,58	5,80	6,02	6,70	6,92	7,71	7,98	6,96	8,08	8,54	6,90
La/Ta	28,57	30,00	33,33	15,00	15,79	25,00	31,25	25,00	15,00	25,00	11,11	12,50	15,79	16,67	27,27	30,00	1,50	26,32	15,38	28,57	20,00	10,00
La/Nb	1,67	1,60	1,88	0,72	0,73	1,27	1,42	1,44	1,36	1,27	0,53	0,56	0,77	0,75	1,88	1,86	1,34	1,54	0,94	1,52	1,18	1,28
Zr/Ba	0,54	0,28	0,38	0,31	0,32	0,58	0,30	0,44	0,30	0,66	0,26	0,25	0,25	0,29	0,42	0,53	0,46	0,46	0,47	0,54	0,49	0,39
Mg#	23,24	19,01	12,37	48,47	48,51	18,93	35,05	22,30	20,52	38,00	53,89	51,17	48,31	48,67	26,79	11,09	6,70	15,45	11,54	8,03	7,61	21,38

Fig. 5. (a) Rock classification (Le Bas et al., 1986), (b) AFM diagram (Irvine and Baragar, 1971) and (c) K_2O vs. SiO_2 diagram (Peccerillo and Taylor, 1976).

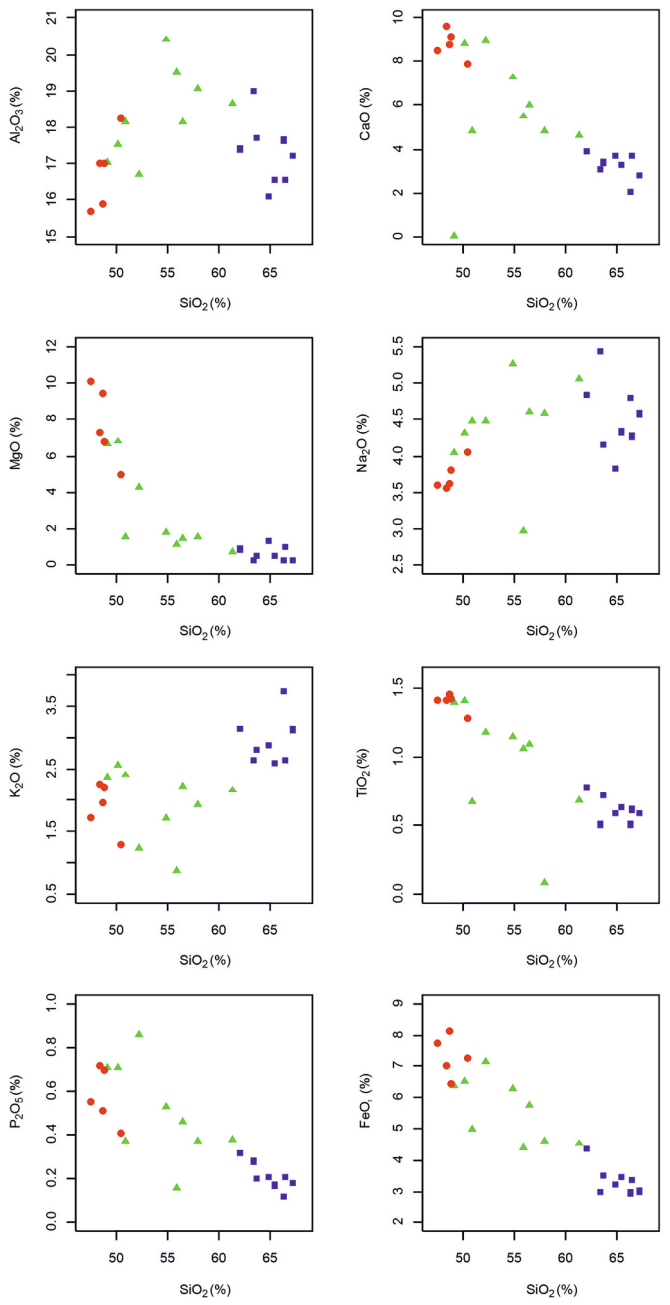

Fig. 6. Selected Harker variation diagrams of major oxides vs. SiO_2 for the GVP volcanics (symbols as in Fig. 5).

8.1. *Timing of volcanism*

The ages obatained by step-heting $^{40}Ar/^{39}Ar$ dating of two samples from the nortwestern part of the GVP rocks match other limited-ages using K—Ar method for the GVP in literature (Wilson et al., 1997; Tankut et al., 1998). Wilson et al. (1997) yielded ages from Güvem area by K—Ar methods; they are 19.7 to 9.5 Ma. These authors claim that the first cycle began with intermediate lava flows and the pyroclastic activity that accompanied them, and that it progressed into more felsic activity during the early Miocene. The alkali basaltic activity started during the second cycle of late Miocene volcanism. On the other hand, Varol et al. (2014) found different K—Ar ages 22.5 to 14.3 Ma for Çamlıdere area, whereas Keller et al.(1992) reported K—Ar ages of 20 Ma and 9.5 Ma for basalts and andesites from Orta area. Although there is some overlap between these studies, these results did not provide good constraints for the volcanism-timing of the GVP.

Previosly published data (mentioned above) belongs to the southern and central parts of the GVP and indicate that the volcanic activitiy occurred between 22.5 ± 0.5 to 9.51 ± 0.3 (Aquitanian to Tortonian) by gained K—Ar method. In previous works, the younger ages probably the volcanism has been extended to around 9 Ma. The Ar/Ar method has advantages increases both the accuracy and precision of the $^{40}Ar/^{39}Ar$ method over the conventional K—Ar techniques. For the first time, in this study, geochronological analyzes were performed by Ar/Ar method to constrain the timing of volcanism in the northen part, previously unstudied area, of the GVP. Ar/Ar dates from the two samples most likely show that volcanism occurred at the earliest Miocene, or around 21 Ma. Previously published K—Ar and our Ar—Ar results are very close to 22 and 21 Ma respectively for the beggining of the volcanism in this province (Fig. 4).

8.2. *Petrogenesis and crystallization processes*

For the origin of intermediate to felsic arc-related magmas, two petrogenetic models were asserted: (1) they derive from mantle-derived basaltic parental magmas by fractional crystallization or assimilation and fractional crystallization (AFC) processes and (2) may result from partial melting of mafic to intermediate igneous sources (Özdamar, 2016 references therein). The studied volcanic rocks were variably altered after eruption, consistent with LOI mostly <3.4% except for one sample. The major elements and the LILEs, such as Na_2O, K_2O, Rb, Sr and Ba, could be mobile during alteration process. Homogeneous Sr—Nd isotopic compositions suggest that the volcanics suffered insignificant post-eruptional alteration (Fig. 8a-d). The examined samples exhibit negative correlations in the $^{143}Nd/^{144}Nd_{(i)}$ vs. $^{87}Sr/^{86}Sr_{(i)}$ plot (Fig. 8a-d), plotting on the mantle array's extension towards the field for upper continental crust but away from the field for lower continental crust.

High CaO values (up to 9.64%) of the andesite and basalt samples indicates amphibole, pyroxene and plagioclase compositions. Fe_2O_3 and MgO contents in volcanics, especially basalts, indicate Fe—Mg silicate minerals (Table 2). They have high Ba between 290 and 790 ppm, and Sr contents between 372 and 1225 ppm (Table 3), considering crustal contamination (Fowler et al., 2008). The samples also have low trace element contents and exhibit a homogeneous distribution, suggesting a similar source for the volcanics. Considering CaO, MgO, TiO_2, P_2O_5 and FeO_T variations with increasing SiO_2 (Fig. 6) show negative good correlations, consistent with derivation of the more silica-rich magmas by crystal fractionation from a more mafic parent magma (Fowler et al., 2008). Non-obvious Eu anomaly suggests minimal amounts of low-pressure plagioclase fractionation (Fig. 7). Low and erratic compatible element levels in the basalt-trachytes, such as those of Cr, Ni, V, and Sc, suggest that mafic minerals may have fractionated in the magma chamber or on their way to the surface (Fig. 9). Their low Cr and Ni levels and the positive association between $Mg^{\#}$ and Cr and Ni might be attributed to olivine and pyroxene fractionation and low Sc (2–17 ppm) content could be fractional crystallization of clinopyroxene (Li et al., 2013). Fractionation of these minerals will raise the La/Tb ratio because Tb has a greater partition coefficient in clinopyroxene and amphibole than La does (Bacon and Druitt, 1988). On a SiO_2(%) vs. La/Tb plot, the basalt to trachytes of the GVP exhibit a straight trend, indicating fractionation of clinopyroxene and amphibole (Fig. 10a). The rocks also exhibit a significant linear trend between Zr/Sm and SiO_2 (%), suggesting that amphibole crystallized fractionally during the transition from primitive basaltic magma to andesitic magma and before the andesitic magma to trachytic magma (Fig. 10b; Leake et al., 1997; Zhang et al., 2014). Conversely, MgO and Fe_2O_3total exhibit a positive association when Fe_2O_3total exceeds 6.0%, but this link vanishes when Fe_2O_3total falls below 6.0% (Fig. 10c). According to all of these findings, fractionation of olivine and clinopyroxene was prevalent in the early stage of magma formation, but amphibole, plagioclase, and clinopyroxene fractionation was more significant in the middle stage (andesitic

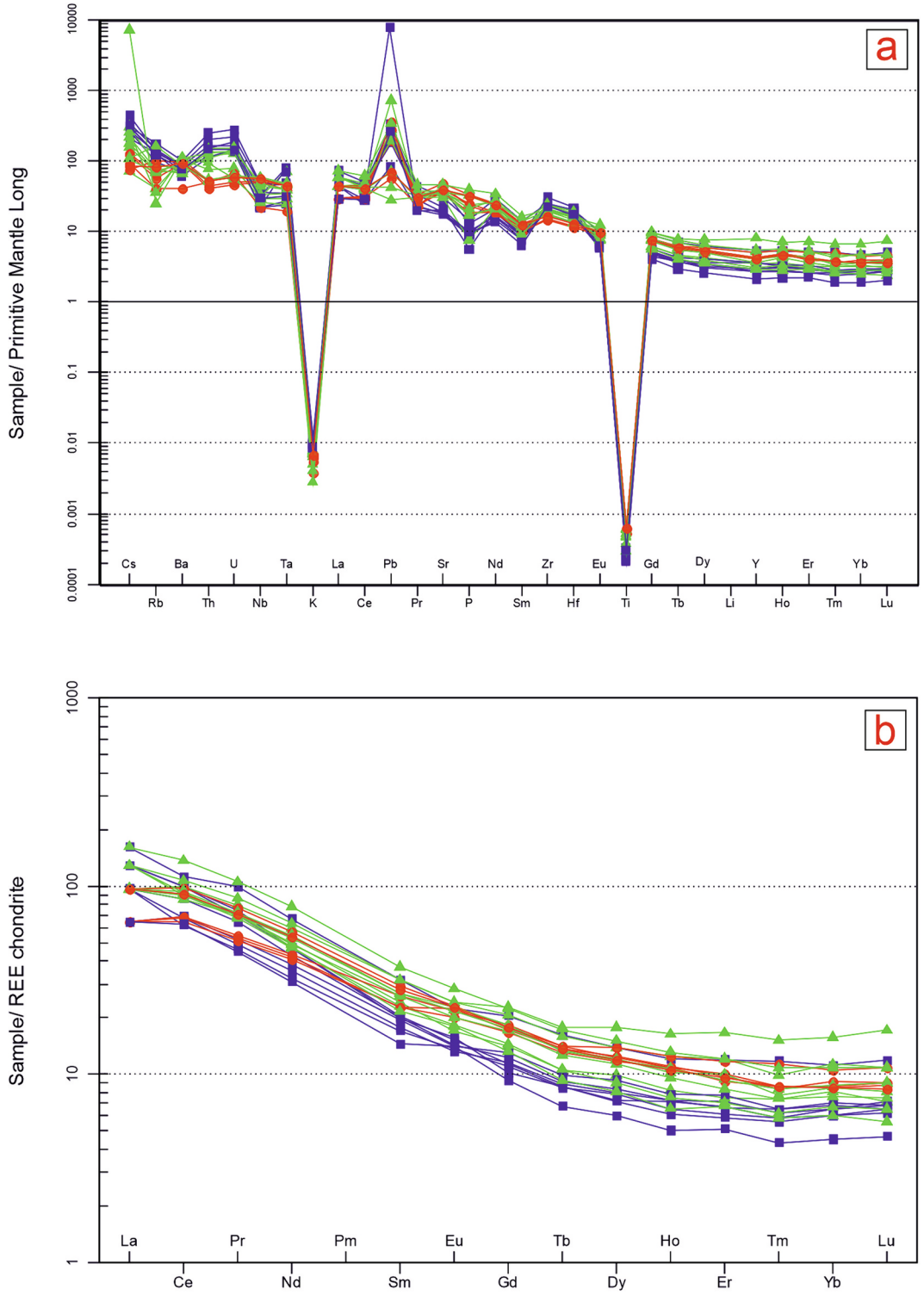

Fig. 7. (a) Primitive mantle-normalized trace element and (b) chondrite-normalized rare earth element patterns of the GVP volcanics (normalizing values from Sun and McDonough (1989) (a) and Boynton (1984) (b) (symbols as in Fig. 5).

Table 4
Whole rock Sr—Nd isotopic data from the Bolu volcanics.

Sample Nr.	SiO_2	Age	Sr	Rb	Sm	Nd	$^{87}Rb/^{86}Sr$	$^{87}/^{86}Sr$	$^{87}/^{86}Sr$ (i)	$^{147}Sm/^{144}Nd$	$^{143}/^{144}Nd$	$^{143}/^{144}Nd(i)$	eNd(T)	eNd(0)
6	65,40	20,39	372	81,9	3,32	19,5	0,6368	0,705,182	0,704,998	0,1034	0,512,687	0,512,673	1,2	1,0
9	57,90	19,07	839	43,7	4,49	27,9	0,1507	0,705,006	0,704,965	0,0977	0,512,711	0,512,699	1,7	1,4
71	54,80	19,07	1070	26,3	6,16	36	0,0711	0,704,638	0,704,619	0,1039	0,512,768	0,512,755	2,8	2,5
72	66,50	20,39	383	84,2	3,81	22,8	0,6359	0,705,171	0,704,987	0,1015	0,512,699	0,512,685	1,4	1,2

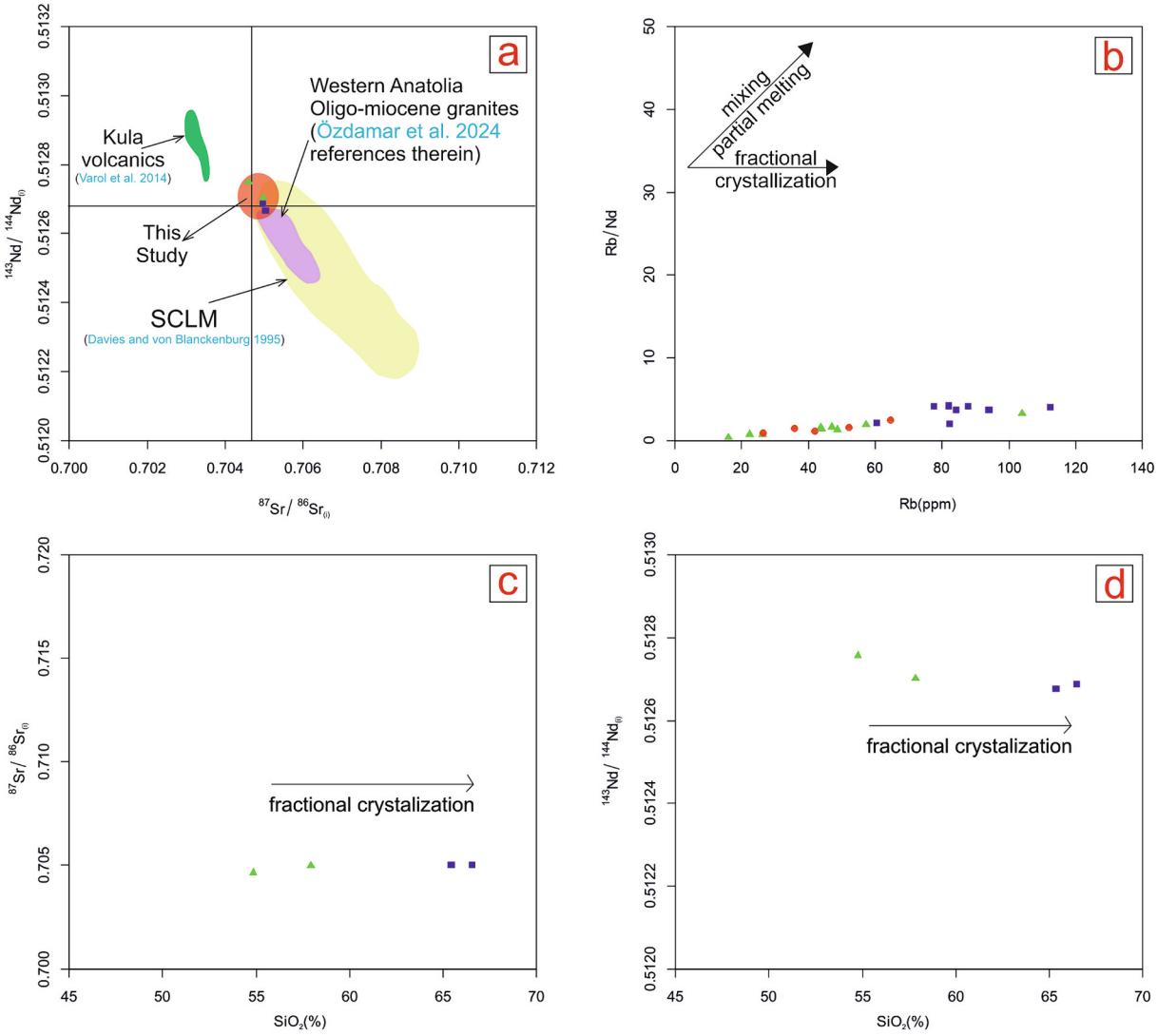

Fig. 8. (a) Average isotope ratios of Sr and Nd of the GVP volcanics (the Western Anatolia Oligo-miocene granites after Özdamar et al. (2024); the SCLM after Davies and von Blanckenburg (1995) and the Kula volcanics after Varol et al. (2014); symbols as in Fig. 5) (b) Rb vs. Rb/Nd diagram, (c) initial ($^{87}Sr/^{86}Sr$) vs. SiO_2 and (d) initial ($^{143}Nd/^{144}Nd$) vs. SiO_2 diagrams of the GVP samples.

magma). Perthite, orthoclase, and quartz-rather than mafic minerals-constrained the magma's evolution as the andesitic magma transformed into silicic magma (Zhang and Gan, 2022 references therein).

To assess the importance of fractional crystallization (FC) or assimilation-fractional crystallization (AFC) processes, we used initial Sr and Nd isotope ratios vs. SiO_2 and trace elements ratios. Despite both positive and negative patterns pointing to AFC processes in the magma, significant FC is indicated by the practically consistent trends. Positive and negative trends indicate AFC processes in the magma, whereas the nearly constant trends indicate significant FC. Fig. 8c, d demonstrates how similar sources were melted to create the volcanics from GVP and how both AFC and FC had an impact on the resulting magmas to account for compositional variations. High La/Ta ratios (11.11–33.33) of the samples that the volcanics derived from the lithospheric mantle source (Thompson and Morrison, 1988). Besides, high La/Nb and low Zr/Ba ratios indicate a lithospheric mantle source (DePaolo and Daley, 2000; Menzies et al., 1991).

Pearce (1983) asserted that Th/Yb versus Nb/Yb diagram can be used for the detection of crustal signatures in the magmas that have interacted with continental crust during its ascent, or could have a subduction component when they are displaced to higher Th/Yb values. In this diagram, the GVP samples plot within mantle array, upper crust and volcanic arc fields (Fig. 11a). In Fig. 11b,c, the samples show crustal or sediments contamination (Woodhead and Hergt, 2001; Keppler, 1996; Stolper and Newman, 1994; Lambert and Holland, 1974). The studied samples display enrichment in LIL elements and are depleted in HFS elements, impliying that they may have been produced as a result of subduction mechanism and/or crustal contamination during the ascent of the magma to the surface (Arculus, 1994).

The Early Miocene eruption ages of the andesite (A71) and trachyte (T6) samples are similar, suggesting that the basic and felsic volcanics erupted ca.21 Mys ago. Additionally, the identical LREE levels and virtually flat REE distribution patterns of these basic to intermediate volcanics (Fig. 7) point to the same magma source as the origin of these rocks. The fact that there is no discernible difference in the ratios of highly incompatible elements (such as Nb/Th vs. Ta/Th) between the basalts and the other volcanic rocks in the study area (Fig. 11c) also supports this theory (Keppler, 1996). On Lambert and Holland (1974) Y vs. CaO diagram, which is depicted as a J-type trend, all the rocks are found to plot on the Y depleted side of the typical calc-alkaline trend (Fig. 11d). This pattern suggests that pyroxene, plagioclase, and hornblende were crucial to the development of the GVP volcanics. These volcanic rocks were generated by partial melting of an incompatible element enriched, subduction-modified, mantle source linked to the

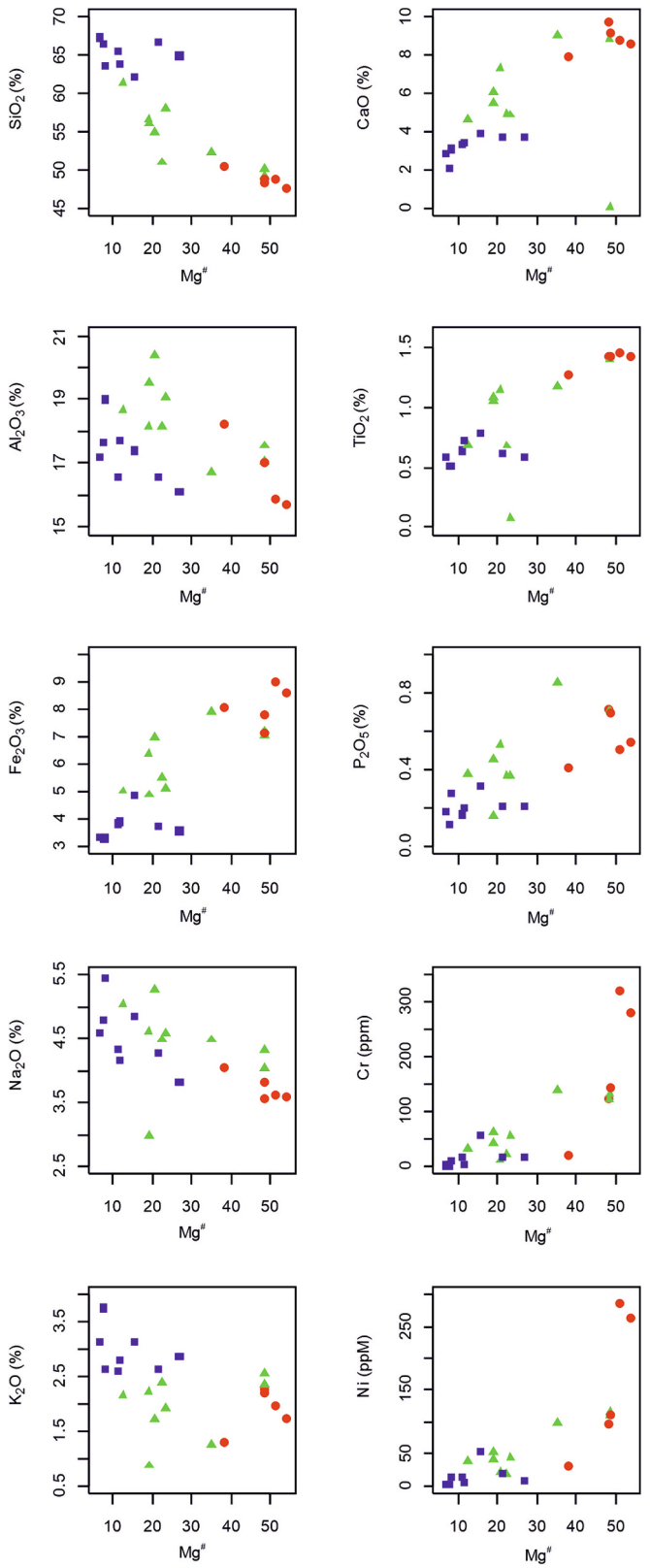

Fig. 9. Selected Harker variation diagrams of major oxides and trace elements vs. $Mg^{\#}$ for the GVP volcanics (symbols as in Fig. 5).

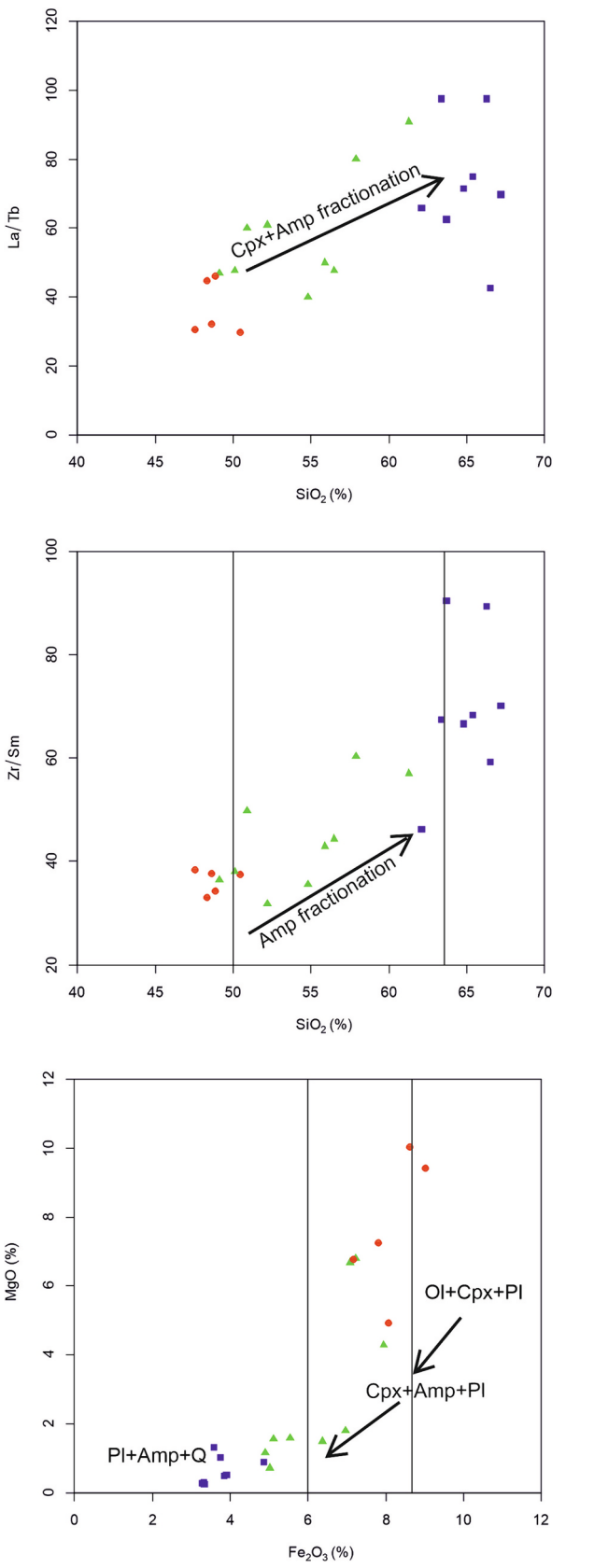

Fig. 10. (a) La/Tb vs. SiO_2 diagram (Schiano et al., 2010), (b) Zr/Sm vs. SiO_2 diagram (Schiano et al., 2010) and (c) MgO vs. Fe_2O_3 diagram (symbols as in Fig. 5).

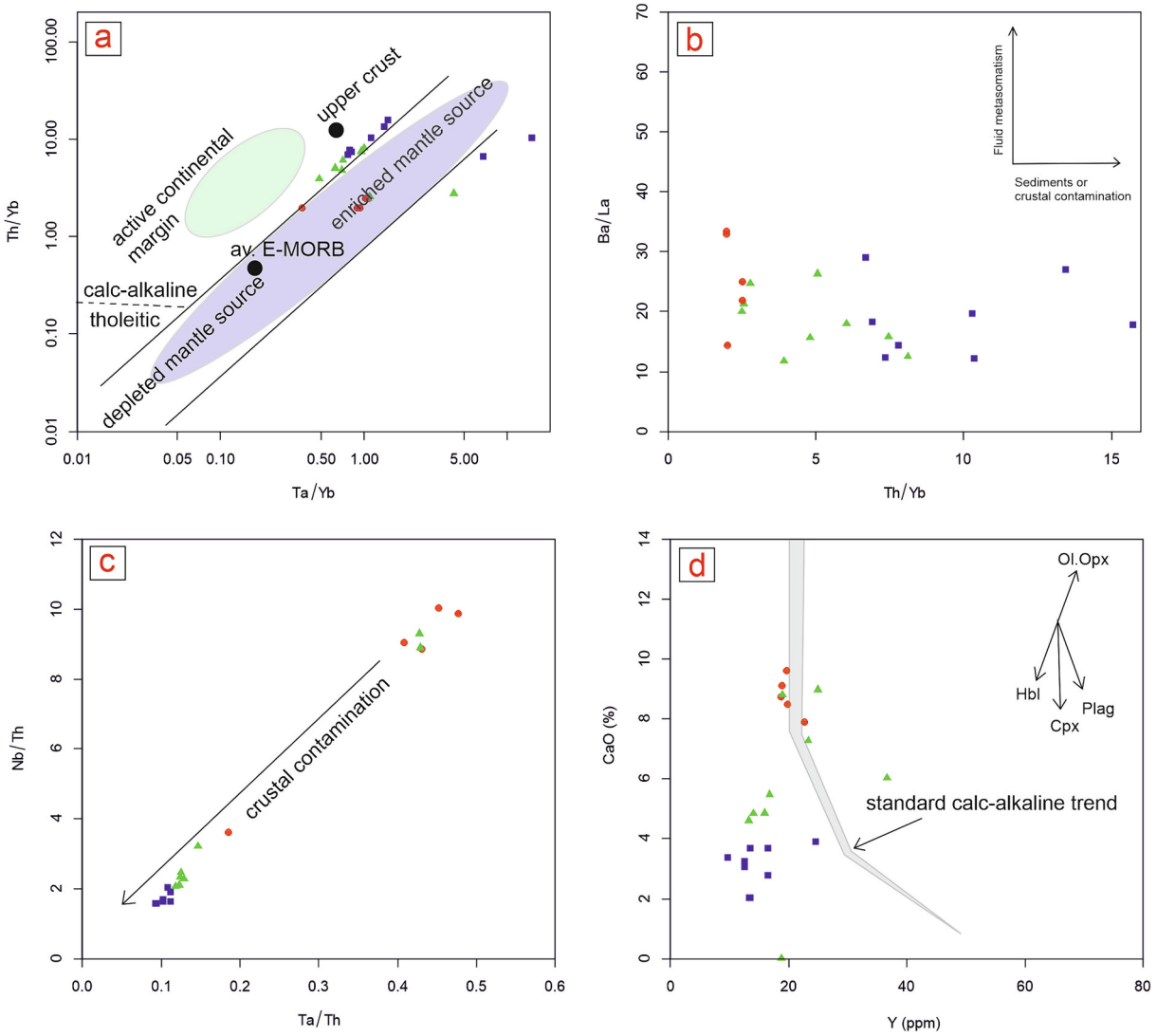

Fig. 11. (a) Th/Yb vs. Ta/Yb diagram (Pearce, 1983), (b) Ba/La vs. Th/Yb diagram (Woodhead and Hergt, 2001), (c) Nb/Th vs. Ta/Th diagram (Keppler, 1996; Stolper and Newman, 1994) and (d) CaO vs. Y (ppm) diagram (Lambert and Holland, 1974). (symbols as in Fig. 5).

northward subduction of the northern branch of the Neo-Tethys.

8.3. Tectonic setting

Late Mesozoic to Cenozoic geological evolution of Anatolia is closely related to opening and closure of the Neotethys Ocean. After the Late Triassic opening of the Neotethys Ocean, it started to close by northward subduction during Late Cretaceous (Şengör and Yilmaz, 1981; Özdamar et al., 2012). The İzmir-Ankara-Erzincan and Inner Tauride Suture zones represent remnants of the Ocean's Northern Branch following the Eocene collision of Tauride-Anatolide block with the Pontides and the Central Anatolia Crystalline Complex (CACC). Unlikely, the closure of the Southern Branch of the Neotethys is still subducting under the Taurides along to the contemporary Cyprus subduction zone in the Mediterranean (Koç et al., 2012). The authors have claimed that this subduction zone has been in retreat relative to the Central Anatolia since the Miocene in extension-related volcanism. Central Anatolia hosts several post-collisional volcanic provinces and complexes (e.g., Galatia Volcanic Province and the Cappadocian Volcanic Province. In the GVP, Early to Middle Miocene activity consists of large volumes of calc-alkaline intermediate and felsic rocks with small volumes of mildly alkaline mafic to intermediate lavas. The volcanic rocks of GVP display geochemical characteristics of both subduction-related and intraplate magmatism (Varol et al., 2014).

The studied samples from GVP plot in the arc volcanic field and the active continental margin field (Fig. 11a), characterized by calc-alkaline affinity (Fig. 5b). The GVP samples display negative anomalies in Nb and Ti that the most typical feature for the arc magmatism (Fitton et al., 1988; Kempton et al., 1991). The samples plot either in or close to the arc volcanic subfield on the Nb/Th vs Nb diagram of Dilek et al., 2010 (Fig. 12a). The basalt samples of GVP, in particular, lie inside the plate basalt field on the Ti/100–Zr ppm)–Y x 3 (Pearce and Cann, 1973) discrimination map employing immobile minor and trace elements (Fig. 12b). These diagrams are applicable to basalts, intermediate, and felsic rocks; they are particularly helpful in differentiating amongst arc volcanic rocks (Wood et al., 1979). On the Th–Hf/3–Nb/16 discrimination diagram of Wood (1980) using immobile minor and trace elements, the samples fall in the field of arc volcanic setting and calc-alkaline basalt (Fig. 12c).

Most of the samples exhibit typical characteristics of subduction-related magmatic activity with LIL elements enrichment, HFS elements depletion and high initial $^{87}Sr/^{86}Sr$ and low initial $^{143}Nd/^{144}Nd$ isotope ratios. Their high La/Nb ratio and high La/ Ta ratios indicate that they were generated from a lithospheric mantle source. Taking into account all of the available data, we think that the magmatic activity was generated from a lithospheric mantle as a result of crustal extension

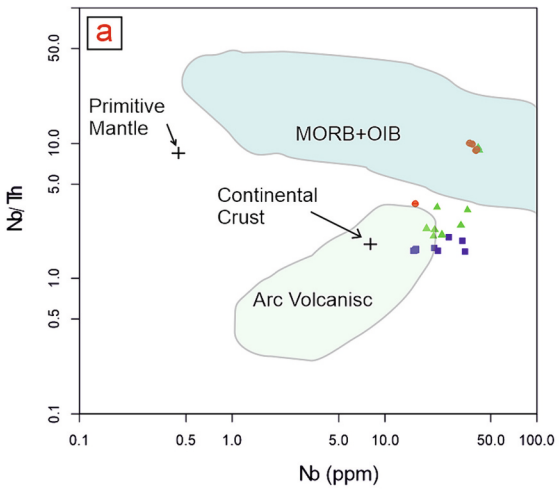

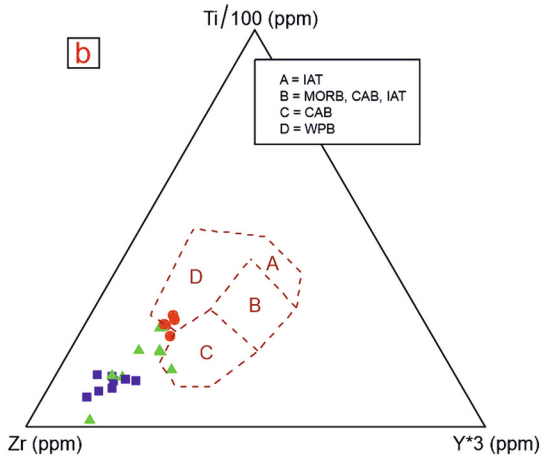

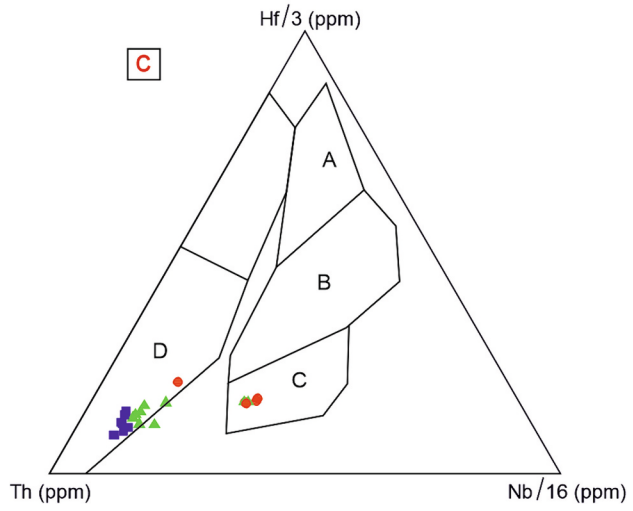

Fig. 12. (a) Nb/Th vs. Nb (ppm) diagram, (b) Zr (ppm)-Ti/100 (ppm9-Y*3 (ppm) ternary diagram (Pearce and Cann, 1973) and (c) Th (ppm)-Hf/3 (ppm)-Nb/16 (ppm) ternary diagram (A: N-MORB; B: *E*-MORB and within plate tholeiitic basalt; C: within plate alkaline basalt; D: within volcanic arc basalt; Primitive Mantle from (Hofmann, 1988). (a) The volcanic arc field from Jahn and Zhang (1984), the primitive mantle value from Sun and McDonough (1989), the mean continental crust value from Taylor and McLennan (1985) and Condie (1993), and field of MORB+OIB were taken from Schmidberger and Hegner (1999) (symbols as in Fig. 5).

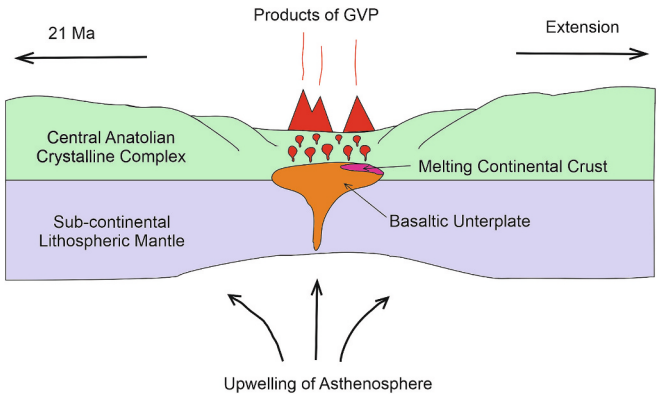

Fig. 13. Geodynamic model for the Miocene-aged Galatia Volcanic Province (GVP) in the Central Anatolia.

of the Neotethys fits for the tectonic setting of the GVP (Fig. 13).

9. Conclusions

We arrived following conclusions based on new results combined with the previously published data:

1. The GVP hosts volcanic rocks, including basalt, andesite, trachy-andesite, trachyte and their pyroclastics. The rocks display similar petrographic characteristics with little diversity, having porphyritic, intergranular and ophitic texture except for pyroclastics.
2. The volcanic activity took place in the earliest Miocene at ca. 21 Ma (Aquitanian).
3. Magmatic activity, resulted in Miocene volcanism, was generated from a lithospheric mantle in an extensional setting as a result of crustal extension of the Neotethys.
4. Initial ($^{87}Sr/^{86}Sr$) and ($^{143}Nd/^{144}Nd$) values indicate that fractional crystallization processes and crustal contamination affected the mantle-originated primary magma.

CRediT authorship contribution statement

Şenel Özdamar: Writing – review & editing, Writing – original draft, Conceptualization. **Mehmet Z. Billor:** Methodology, Data curation. **Oral Sarıkaya:** Software, Methodology, Data curation. **Bala Ekinci Şans:** Writing – original draft, Software. **Taşkın Deniz Yıldız:** Software, Methodology, Data curation. **Fahri Esenli:** Methodology, Data curation. **Haibo Zou:** Writing – review & editing, Methodology, Data curation. **Sarah Sherlock:** Writing – review & editing, Methodology. **Ali Haydar Gültekin:** Writing – original draft, Software.

Declaration of competing interest

The authors declare that they have no known competing financial interests or personal relationships that could have appeared to influence the work reported in this paper.

Data availability

Data will be made available on request.

Acknowledgments

The first author received financial support Istanbul Technical University (ITU-BAP). The authors are grateful to editor and two anonymous reviewers for excellent suggestions and critical comments, which improved the scientific content.

References

Arculus, R.J., 1994. Aspects of magma genesis in arcs. Lithos 33 (1–3), 189–208.

Bacon, C.R., Druitt, T.H., 1988. Compositional evolution of the zoned calcalkaline magma chamber of Mount Mazama, Crater Lake, Oregon. Contrib. Mineral. Petrol. 98, 224–256.

Boynton, W.V., 1984. Cosmochemistry of the rare earth elements: meteorite studies. In: Henderson, R. (Ed.), Rare Earth Element Geochemistry. Developments in Geochemistry, 2. Elsevier, pp. 89–92.

Condie, K.C., 1993. Chemical composition and evolution of the upper continental crust: contrasting results from surface samples and shales. Chem. Geol. 104 (1–4), 1 37.

Davies, J.H., von Blanckenburg, F., 1995. Slab breakoff: a model of lithosphere detachment and its test in the magmatism and deformation of collisional orogens. Earth Planet. Sci. Lett. 129 (1–4), 85–102.

DePaolo, D.J., Daley, E.E., 2000. Neodymium isotopes in basalts of the southwest basin and range and lithospheric thinning during continental extension. Chem. Geol. 169, 157–185.

Dilek, Y., Imamverdiyev, N., Altunkaynak, S., 2010. Geochemistry and tectonics of Cenozoic volcanism in the Lesser Caucasus (Azerbaijan) and the peri-Arabian region: collision-induced mantle dynamics and its magmatic fingerprint. Int. Geol. Rev. 52 (4–6), 536–578.

Fitton, J.G., James, D., Kempton, P.D., Ormerod, D.S., Leeman, W.P., 1988. The role of lithospheric mantle in the generation of late Cenozoic basic magmas in the Western United States. J. Petrol. Spec. Issue 331–349.

Fourquin, C., Paicheler, J.C., Sauvage, J., 1970. Premieres données sur la stratigraphie du Massif Galate d'andesites, étude palynologique de la base des diatomites Miocenes de Beçkonak au Nord-Est de Kizilcahamam (Anatolie Turquie). Comp. Rendu Ac. Sc. D270, 2253–2255.

Fowler, M.B., Kocks, H., Darbyshire, D.P.F., Greenwood, P.B., 2008. Petrogenesis of high Ba–Sr plutons from the northern highlands Terrane of the British Caledonian Province. Lithos 105 (1–2), 129–148.

Gökten, E., Özaksoy, V., Karakuş, K., 1996. Tertiary Volcanic and Tectonic Evolution of the Ayaş-Güdül-Çeltikçi Region, Turkey. Int. Geol. Rev. 38, 926–934.

Hofmann, A.W., 1988. Chemical differentiation of the Earth: the relationship between mantle, continental crust and oceanic crust. Earth Planet. Sci. Lett. 90, 297–314.

Irvine, T.N., Baragar, W.R.A., 1971. A guide to the chemical classification of the common volcanic rocks. Can. J. Earth Sci. 8 (5), 523–548.

Jahn, B.M., Zhang, Z.Q., 1984. Archean granulite gneisses from eastern Hebei Province, China: rare earth geochemistry and tectonic implications. Contrib. Mineral. Petrol. 85, 224–243.

Keller, J., Jung, D., Eckhardt, F.-J., Kreuzer, H., 1992. Radiometric ages and chemical characterization of the Galatean andesite massif, Pontus, Turkey. Acta Vulcanol. 2, 267–276.

Kempton, P.D., Fitton, J.G., Hawkesworth, C.J., Ormerod, D.S., 1991. Isotopic and trace element constraints on the composition and evolution of the lithosphere beneath the Southwestern United States. J. Geophys. Res. 96 (B8), 13713–13735.

Keppler, H., 1996. Constraints from partitioning experiments on the composition of subduction-zone fluids. Nature 380 (6571), 237–240.

Koç, A., Kaymakci, N., van Hinsbergen, D.J.J., Kuiper, K.F., Vissers, R.L.M., 2012. Tectono sedimentary evolution and geochronology of the middle Miocene Altınapa basin, and implications for the late Cenozoic uplift history of the Taurides, southern Turkey. Tectonophysics 532e535, 134e155.

Lambert, R.S.J., Holland, J.G., 1974. Yttrium geochemistry applied to petrogenesis utilizing calcium-yttrium relationships in minerals and rocks. Geochim. Cosmochim. Acta 38 (9), 1393–1414.

Le Bas, M.J., Maitre, R.L., Streckeisen, A., Zanettin, B., IUGS Subcommission on the Systematics of Igneous Rocks, 1986. A chemical classification of volcanic rocks based on the total alkali-silica diagram. J. Petrol. 27 (3), 745–750.

Leake, B.E., Woolley, A.R., Arps, C.E.S., Birch, W.D., Gilbert, M.C., Grice, J.D., Hawthorne, F.C., Kato, A., Kisch, H.J., Krivovichev, V.G., Linthout, K., Laird, J., Mandarino, J.A., Maresch, W.V., Nickel, E.H., Rock, N.M.S., Schumacher, J.C., Smith, D.C., Stephenson, N.C.N., Ungaretti, L., Whittaker, E.J.W., Youzhi, G., 1997. Nomenclature of the amphiboles: Report of the subcommittee on amphiboles of the International Mineralogical Association, Commission on New Minerals and Mineral Names. Am. Mineral. 82, 1019–1037.

Lee, J.K., Marti, K., Severinghaus, J.P., Kawamura, K., Yoo, H.S., Lee, J.B., Kim, J.S., 2006. A redetermination of the isotopic abundances of atmospheric Ar. Geochim. Cosmochim. Acta 70, 4507–4512.

Li, C.F., Li, X.H., Li, Q.L., Guo, J.H., Yang, Y.H., 2012. Rapid and precise determination of Sr and Nd isotopic ratios in geological samples from the same filament loading by thermal ionization mass spectrometry employing a single-step separation scheme. Anal. Chim. Acta 727, 54–60.

Li, Y., He, J., Wang, C., Santosh, M., Dai, J., Zhang, Y., Wei, Y., Wang, J., 2013. Late cretaceous K-rich magmatism in Central Tibet: evidence for early elevation of the Tibetan plateau? Lithos 160-161, 1–13.

Menzies, M.A., Kyle, P.R., Jones, M., Ingram, G., 1991. Enriched and depleted source components for tholeiitic and alkaline lavas from Zuni-Bandera, New Mexico: ınferences about intraplate processes and stratified lithosphere. J. Geophys. Res. 96 (B8), 13645–13671.

Özdamar, Ş., 2016. Geochemistry and geochronology of late Mesozoic volcanic rocks in the northern part of the Eastern Pontide Orogenic Belt NE Turkey: implications for the closure of the Neo Tethys Ocean. Lithos 248, 240–256.

Özdamar, Ş., Roden, M.F., Esenli, R.F., Uz, B., Wampler, J.M., 2012. Geochemical features and K Ar age data from metadetrital rocks and high K metasomatized metarhyolites in the Afyon Bolkardağ Zone Ilgin Konya SW Turkey. Neues Jahrbuch für Mineralogie - Abhandlungen 189 (2), 155–176.

Özdamar, Ş., Zou, H., Billor, M.Z., Hames, W., Roden, M.F., Sarıkaya, O., Georgiev, S., 2024. Petrogenesis, geochronology and thermochronology of Oligocene to Miocene Western Anatolia granitoid plutons in Turkey. Lithos 464, 107430.

Pearce, J.A., 1983. Role of the sub-continental lithosphere in magma genesis at active continental margins. In: Hawkesworth, C.J., Norry, N.J. (Eds.), Continental Basalts and Mantle Xenoliths. Shiva, Cheshire, UK, pp. 230–249.

Pearce, J.A., Cann, J.R., 1973. Tectonic setting of basic volcanic rocks determined using trace element analyses. Earth Planet. Sci. Lett. 19 (2), 290–300.

Pearce, J.A., Parkinson, I.J., 1993. Trace element models for mantle melting: application to volcanic arc petrogenesis. Geol. Soc. Lond. Spec. Publ. 76 (1), 373–403.

Pearce, J.A., Harris, N.B., Tindle, A.G., 1984. Trace element discrimination diagrams for the tectonic interpretation of granitic rocks. J. Petrol. 25 (4), 956–983.

Peccerillo, R., Taylor, S.R., 1976. Geochemistry of Eocene calc-alkaline volcanic rocks from the Kastamonu area, northern Turkey. Contrib. Mineral. Petrol. 58, 63–81.

Renne, P.R., Balco, G., Ludwig, K.R., Mundil, R., Min, K., 2011. Response to the comment by W.H. Schwarz et al. on "Joint determination of ^{40}K decay constants and $^{40}Ar^*/^{40}K$ for the fish Canyon sanidine standard, and improved accuracy for $^{40}Ar/^{39}Ar$ geochronology" by P.R. Renne et al., 2010. Geochim. Cosmochim. Acta 75, 5097–5100.

Şahinci, A., 1975. Ilıca Köyü Çevresi jeoloji- Hidrojeoloji Etüdü. MTA Dergisi, Ankara, pp. 46–61.

Schiano, P., Monzier, M., Eissen, J.P., Martin, H., Koga, K.T., 2010. Simple mixing as the major control of the evolution of volcanic suites in the Ecuadorian Andes. Contrib. Mineral. Petrol. 160, 297–312.

Schmidberger, S.S., Hegner, E., 1999. Geochemistry and isotope ststematics of calc-alkaline volcanic rocks from the Saar-Nahe basin (SW Germany)- implications for late Variscan orogenic development. Contrib. Mineral. Petrol. 135, 373–385.

Schumacher, R., Mues-Schumacher, U., Toprak, V., 2001. The Sarikavak Tephra, Galatea, north Central Turkey: a case study of a Miocene complex plinian eruption deposit. J. Volcanol. Geotherm. Res. 112 (1–4), 231–245.

Şengör, A.C., Yilmaz, Y., 1981. Tethyan evolution of Turkey: a plate tectonic approach. Tectonophysics 75 (3–4), 181–241.

Staudigel, H., Yayanos, A., Chastain, R.A., Bourcier, R., Boucier, R., 1995. Biologically mediated dissolution of glass. Chem. Geol. 126, 147–154.

Stolper, E., Newman, S., 1994. The role of water in the petrogenesis of Mariana trough magmas. Earth Planet. Sci. Lett. 121 (3–4), 293–325.

Sun, S.S., McDonough, W.F., 1989. Chemical and isotope systematics of oceanic basalts; implication for mantle compositions and processes. In: Saunders, A.D., Nory, M.J. (Eds.), Magmatism in the Ocean Basins, Geological Society of London, Special Publication, vol. 42, pp. 313–345.

Tanaka, T., Togashi, S., Kamioka, H., Amakawa, H., Kagami, H., Hamamoto, T., Yuhara, M., Orihashi, Y., Yoneda, S., Shimizu, H., Kunimaru, T., Takahashi, K., Yanagi, T., Nakano, T., Fujimaki, H., Shinjo, R., Asahara, Y., Tanimizu, M., Dragusanu, C., 2000. JNdi-1: a neodymium isotopic reference in consistency with LaJolla neodymium. Chem. Geol. 168 (3), 279–281.

Tankut, A., 1990. Ankara Ofiyolitli Melanj Kuşağı İçindeki Ofiyolitik Kayaçların Tektonik Oluşum Ortamlarına Jeokimyasal Bir Yaklaşım MTA Dergisi, 110, pp. 17–28.

Tankut, A., Dilek, Y., Önen, P., 1998. Petrology and geochemistry of the Neo-Tethyan volcanism as revealed in the Ankara Melange, Turkey. J. Volcanol. Geotherm. Res. 85, 265–284.

Taylor, S.R., McLennan, S.M., 1985. The continental crust. In: Its Composition and Evolution. Blackwell, Oxford, p. 312.

Thompson, R.N., Morrison, M.A., 1988. Asthenospheric and lower-lithospheric mantle contributions to continental extensional magmatism: an example from the British Tertiary Province. Chem. Geol. 68 (1–2), 1–15.

Toori, M., 2005. Orhaniye ve Civarının (KKB Ankara-Türkiye) Neojen Stratigrafisi ve Tektoniği. In: Yüksek Lisans Tezi, Hacettepe Üniversitesi Fen Bilimleri Enstitüsü, Ankara, 76s, p. 65.

Toprak, V., Savaşçın, Y., Güleç, N., Tankut, A., 1996. Structure of the Galatean Province. Int. Geol. Rev. 38, 747–758.

Türkecan, A., 1991. Petrology of the Pliocene Volcanics around Muş SE, Anatolia. Bull. Min. Res. Explor. 112, 85–101.

Varol, E., Temel, A., Gourgaud, A., 2008. Textural and compositional evidence for magma mixing in the evolution of the Camlıdere Volcanic Rocks (Galatean Volcanic Province), Central Anatolia, Turkey. Turk. J. Earth Sci. 17 (4), 709–727.

Varol, E., Temel, A., Yürür, T., Gourgaud, A., Bellon, H., 2014. Petrogenesis of the Neogene bimodal magmatism of the Galatean volcanic province, Central Anatolia, Turkey. J. Volcanol. Geotherm. Res. 280, 14–29.

Vermeesch, P., 2018. Dissimilarity measures in detrital geochronology. Earth Sci. Rev. 178, 310–321.

Wilson, M., Tankut, A., Guleç, N., 1997. Tertiary volcanism of the Galatia Province, NW Central Anatolia, Turkey. Lithos 42, 105–121.

Wood, D.A., 1980. The application of a Th-Hf-Ta diagram to problems of tectonomagmatic classification and to establishing the nature of crustal contamination of basaltic lavas of the British Tertiary Volcanic Province. Earth Planet. Sci. Lett. 50 (1), 11–30.

Wood, D.A., Tarney, J., Varet, J., Saunders, A.D., Bougault, H., Joron, J.L., Cann, J.R., 1979. Geochemistry of basalts drilled in the North Atlantic by IPOD Leg 49: implications for mantle heterogeneity. Earth Planet. Sci. Lett. 42 (1), 77–97.

Woodhead, J.D., Hergt, J.M., 2001. Strontium, neodymium and lead isotope analyses of NIST glass certified reference materials: SRM 610, 612, 614. Geostand. Newslett. 25 (2–3), 261–266.

Yihunie, T.W., 1993. Geology, Petrography and Geochemistry of Volcanic Rocks from Güvem Area, Kyzylcahamam, Ankara. Unpublished MSc Thesis. Middle East Technical University, Ankara, Turkey.

Zhang, Y., Gan, T., 2022. Diffusion in Melts and Magmas. Rev. Mineral. Geochem. 87 (1), 283–337.
Zhang, L.-Y., Ducea, M.N., Ding, L., Pullen, A., Kapp, P., Hoffman, D., 2014. Southern Tibetan Oligocene–Miocene adakites: A record of Indian slab tearing. Lithos 210–211, 209–223.
Zou, H.B., Zindler, A., Xu, X., Qi, Q., 2000. Major, trace element, and Nd, Sr and Pb isotope studies of Cenozoic basalts in SE China: mantle sources, regional variations and tectonic significance. Chem. Geol. 171, 33–47.